Disorder-induced unbinding of a flux line from an extended defect

Leon Balents
Physics Department, Harvard University, Cambridge, Massachusetts 02138

Mehran Kardar
Physics Department, Massachusetts Institute of Technology, Cambridge, Massachusetts 02139
(Received 19 November 1993)

We study the competition, for a single flux line, between pinning by bulk point randomness and an extended defect, such as an ion track, dislocation line, or twin plane. In three dimensions, there is an unbinding transition for a linear (but not a planar) defect. This transition is analyzed using Flory, Migdal-Kadanoff, functional renormalization-group, and numerical methods. The localization length, describing the typical transverse separation between the vortex line and defect, diverges like $\ell_\perp \sim |T - T_c|^{-\nu_\perp}$, with $\nu_\perp \approx 1.4$. We predict the effects of this localization length on the I-V characteristics of the superconductor, and suggest experiments to observe the transition.

I. INTRODUCTION

It is now well known that fluctuations can drastically change the nature of the Abrikosov phase of type-II superconductors. Thermal disorder can melt the vortex lattice, forming a flux liquid at both low and high vortex densities.[1] Quenched randomness also leads to new behavior,[2] which depends upon its degree of correlation. Point defects, such as vacancies or interstitials, encourage line wandering, and may lead to the formation of a glassy phase with a nonzero critical current, called a vortex glass.[3] More recently, the experimental creation of "columnar," or linear, pinning sites[4,5] has inspired theoretical treatment of the resulting "Bose glass" phase.[6,7] Twin planes, planar defects which occur naturally as a type of grain boundary, lead to a yet different glassy phase.[8]

When both point and extended defects (such as columnar pins or twin boundaries) are present, the theoretical (and experimental) situation is less clear.[9,10] Scaling arguments suggest that the Bose glass phase is unstable to point disorder.[9] Although the vortex glass is itself not well understood, it is quite possible that the addition of correlated disorder leads to an instability in this case as well. At present, the only concrete calculations addressing this problem for bulk systems are renormalization-group analyses in two dimensions,[9] and in a dislocation-free model in $5-\epsilon$ dimensions.[10] The nature of the phase(s) in three dimensions in the presence of dislocations and point defects remains an open question.

Much of the difficulty of the competing-disorder problem derives from the lack of a detailed understanding of the bulk vortex glass phase. The behavior of a single flux line (FL) with point disorder, however, is well understood.[11–13] The equilibrium statistical mechanics of a single FL and a single extended defect is also well known (see, e.g., Ref. 7 or Ref. 14). In this paper, we analyze one FL in the presence of *both* bulk point randomness and a single extended defect (see Fig. 1).[15]

Although both point disorder and the extended defect act to pin the FL, the nature of the pinned state in each case is quite different. With purely point disorder, the FL tends to wander transversely as it proceeds along the magnetic field axis, in order to take advantage of locally favorable regions of impurities. The extended defect, on the other hand, attracts the FL to itself, suppressing wandering. An important characterization of the FL, therefore, is whether it wanders arbitrarily far as its length increases, or whether it remains within some width $\ell_\perp$ of the extended defect. In general, both the former and latter cases are possible, and will be referred to as delocalized and localized phases, respectively.

In three dimensions with a columnar defect, we find

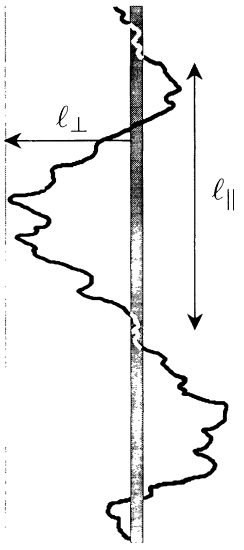

FIG. 1. Flux line localized around a columnar pin in three dimensions ($d = 3$, $n = 1$). White portions of the FL indicate when it is on the defect.

that both localized and delocalized phases exist, provided that the point randomness is sufficiently strong. In this case, the FL is localized at high temperatures, with a second-order unbinding transition as temperature is decreased through some critical point T_u. As the critical temperature is approached from above, the localization length diverges with the power law $\ell_\perp \sim (T - T_u)^{-\nu_\perp}$. The best estimate of the critical exponents is obtained using renormalization-group (RG) techniques, which yield $\nu_\perp \approx 1.4$, in agreement with numerical simulations which yield $\nu_\perp = 1.3 \pm 0.6$. The RG calculation also yields the specific heat exponent $\alpha \approx 0.21$. For a planar defect in three dimensions, the FL is localized at all temperatures. Even at zero temperature, there is a nonzero localization length due to point defects. Experimentally, this behavior may be observed at low magnetic fields and low densities of extended defects.

The outline of the paper is as follows. In Sec. II, we present the appropriate free energy for a single FL, and discuss methods for estimating the magnitudes of its various terms starting from fundamental parameters of the superconductor. Section III describes the phases of the model and analyzes their stabilities. In Sec. IV a characterization of the unbinding transition is given, along with simple "mean-field" or Flory estimates for the critical exponents. In Sec. V, a Migdal-Kadanoff RG is introduced as a first attempt to remedy the deficiencies of the scaling arguments in the previous section. Functional renormalization-group techniques, described in Sec. VI, lead to a controlled expansion for the critical exponents, and the results quoted above. These predictions are tested against numerical simulations in Sec. VII, and show reasonable agreement. In Sec. VIII, we determine the limits of applicability of our theory, evaluate the estimates of Sec. II for several types of point and columnar defects in $YBa_2Cu_3O_7$ (YBCO), and suggest methods of experimental observation of FL delocalization. In Sec. IX, we review our conclusions, the relationship to other work, and give suggestions for future research.

II. MODEL

A. Free energy

Choosing the z axis along the direction of the magnetic induction $\mathbf{B}$, it is natural to describe the conformation of the flux line by a vector $\mathbf{x}(z)$ transverse to this axis. For the sake of generality, we will consider a d-dimensional space, so that $\mathbf{x}(z) \in \Re^{d-1}$, though all numerical estimates will, of course, be calculated in the physical case $d = 3$. The free energy is a modification of that originally introduced by Nelson and Seung,[1]

$$F = \int_0^L dz \left\{ \frac{\tilde{\epsilon}_1}{2} \left| \frac{d\mathbf{x}(z)}{dz} \right|^2 - V_D(\mathbf{x}_\perp(z)) - V_P(\mathbf{x}(z), z) \right\}, \tag{2.1}$$

where $V_D(\mathbf{x}_\perp(z))$ and $V_P(\mathbf{x}(z), z)$ are potentials representing the extended defect and point disorder, respectively. The FL stiffness constant $\tilde{\epsilon}_1$ has been calculated in its full wave-vector-dependent form in Ref. 16. Up to logarithmic prefactors [of $O(1)$ for most physical situations] its limits are

$$\tilde{\epsilon}_1 \approx \begin{cases} \epsilon_0, & \lambda_{ab} q_z \ll 1, \\ \gamma^2 \epsilon_0, & \lambda_{ab} q_z \gg 1, \end{cases} \tag{2.2}$$

where q_z is the wave vector for distortions involving small numbers of impurities, and γ is the anisotropy.

B. Extended defect potential

The extended defect is modeled as an n-dimensional normal region of width c_0, oriented parallel to the z axis (see Fig. 1). For $n = 1$ or $n = 2$, this model describes pinning by a columnar or planar defect, respectively. The resulting potential V_D is a short-range function of the coordinate $\mathbf{x}_\perp(z) \in \Re^{d-n}$ transverse to the defect, with width b_0 and magnitude U_0. The magnitude U_0 is roughly determined by the condensation energy saved in the normal region, and in the Ginzburg-Landau approximation is estimated as (see Ref. 7)

$$U_0 \approx \begin{cases} \epsilon_0 \left[\ln\left(\frac{c_0}{\sqrt{2}\xi_{ab}}\right) + O(1) \right], & \lambda_{ab} \gg c_0 \gg \xi_{ab}, \\ \epsilon_0 c_0^2/(4\xi_{ab}^2), & c_0 \ll \xi_{ab}, \end{cases} \tag{2.3}$$

where ξ_{ab} is the in-plane coherence length, and c_0 is the actual width of the defect. The constant $\epsilon_0 = (\phi_0/4\pi\lambda_{ab})^2$, where $\phi_0 = hc/2e$ is the flux quantum. The $O(1)$ contribution for $\lambda_{ab} \gg c_0 \gg \xi_{ab}$ arises from the core, and may be quantitatively important due to the only logarithmic dependence on c_0/ξ_{ab}. The effective width is given by $b_0 = \max(c_0, \xi_{ab})$.

C. Point impurity potentials

Generally, the potential due to point defects can be represented as a sum of potentials v_i arising from the individual impurities,

$$\int dz V_P(\mathbf{x}(z), z) = \sum_i v_i(\mathbf{x}(z_i) - \mathbf{x}_i), \tag{2.4}$$

where we have made the approximation that the interaction $v_i(\mathbf{x})$ depends on the transverse distance to the defect, valid when the angle between the FL's and the z axis is not too large. Eq. (2.4) leads to the expression

$$V_P(\mathbf{x}, z) = \sum_i v_i(\mathbf{x} - \mathbf{x}_i)\delta(z - z_i) \tag{2.5}$$

for V_P. The range R and strength E_P of $v_i(\mathbf{x})$ can vary considerably, depending upon the type of defect considered. Oxygen vacancies occur at atomic scales and are thought to be a major source of pinning in untwinned bulk high-temperature superconductors. Other types of defects, such as precipitates,[17] might constitute more mesoscopic-scale bulk randomness in some samples. Con-

sider a single impurity, modeled as a sphere of radius r_0. For $r_0 \gg \lambda$, both the core and field gradient energies are saved over a vortex segment of length $2r_0$, so

$$E_P^{r_0 \gg \lambda_{ab}} \approx 2\epsilon_0 r_0[\ln(\lambda_{ab}/\xi_{ab}) + \Xi], \tag{2.6}$$

where $\Xi \approx 0.1$ is the core contribution to the vortex line energy (see, for example, Ref. 18). When $\xi_{ab} \ll r_0 \ll \lambda$, all the core energy but only a fraction of the field energy is saved, leading to

$$E_P^{\xi_{ab} \ll r_0 \ll \lambda_{ab}} \approx 2\epsilon_0 r_0[\ln(r_0/\xi_{ab}) + \Xi]. \tag{2.7}$$

In both of the above cases, the range is $R \approx r_0$. For $r_0 \ll \xi_{ab}$, the naive assumption of purely core pinning within the spherical defect gives the estimate

$$E_P^{r_0 \ll \xi_{ab}} \approx \epsilon_0 \frac{\Xi}{\pi \xi_{ab}^2} \frac{4}{3} \pi r_0^3. \tag{2.8}$$

In this regime, however, the microscopic core structure may become important. Indeed, a BCS-type calculation yields an enhancement of E_P by roughly a factor of ξ_{ab}/r_0.[19] Such a small impurity may reside anywhere within the core, so $R \approx \xi_{ab}$. We will assume, as is usually true, that this range is quite short compared to the typical point defect separation $s_P \equiv \rho_P^{-1/3}$.

For some calculations, it is useful to treat $V_P(\mathbf{x}, z)$ as a Gaussian random potential with the two-point expectation value

$$\langle V_P(\mathbf{x}, z) V_P(\mathbf{x}', z') \rangle \equiv R(\mathbf{x} - \mathbf{x}') \delta(z - z'). \tag{2.9}$$

Naively, one might expect that the sum in Eq. (2.5) would automatically lead to a Gaussian distribution for $V_P(\mathbf{x}, z)$. The central-limit theorem, however, does not apply in this case, since at any given point $(\mathbf{x}, z)$, no more than one term of the sum is typically nonzero (given the assumption $s_P \gg R$). Instead, short FL segments will be pinned by distinct point impurities. On scales much larger than s_P, however, a coarse-grained FL will experience a smoothed-out random potential closely approximating the form of Eq. (2.9). To estimate $R(\mathbf{x})$, we must carry out this coarse graining explicitly.

To observe Gaussian fluctuations, the system must be divided into volumes containing a number of impurities of $O(1)$. Denoting the transverse and longitudinal lengths of the volumes by x_G and z_G,

$$\rho_P x_G^{d-1} z_G \sim 1. \tag{2.10}$$

At high temperatures, thermal fluctuations dominate the physics on these small scales. Application of the equipartition theorem to Eq. (2.1) then gives

$$x_G \sim \left(\frac{T}{\tilde{\epsilon}_1} z_G \right)^{1/2}. \tag{2.11}$$

Equations (2.10) and (2.11) fix the dimensions of the Gaussian volume. Once fluctuations within the box are accounted for, the coarse-grained theory should include a cutoff in z given by $a \sim z_G$. The solution of Eqs. (2.10) and (2.11) is

$$z_G \sim \rho_P^{-\frac{2}{d+1}} \left(\frac{\tilde{\epsilon}_1}{T} \right)^{\frac{d-1}{d+1}}, \tag{2.12}$$

with x_G given by Eq. (2.11). For $d = 3$, this gives a cutoff of $a \sim \sqrt{\tilde{\epsilon}_1/\rho_P T}$. The typical energy fluctuation within one volume is just the energy E_P, averaged over transverse fluctuations of the FL within the volume,

$$E_G \sim E_P \left(\frac{R}{x_G} \right)^{d-1}. \tag{2.13}$$

For FL segments of length z_G, the coarse-grained potential must be chosen to match Eqs. (2.10)–(2.13). In terms of the small-scale parameters, the correlation function between two Gaussian volumes is

$$\langle V_P(\mathbf{x}, z) z_G V_P(\mathbf{x}', z') z_G \rangle \sim E_G^2 f\left(\frac{\mathbf{x} - \mathbf{x}'}{x_G} \right) g\left(\frac{z - z'}{z_G} \right), \tag{2.14}$$

where $f(\boldsymbol{\chi})$ and $g(\chi)$ are short-range functions with both magnitude and range of $O(1)$. Ignoring physics at scales smaller than the cutoff, $g(\chi) \to \delta(\chi)$, leading to

$$\langle V_P(\mathbf{x}, z) V_P(\mathbf{x}', z') \rangle \sim \frac{E_G^2}{z_G} f\left(\frac{\mathbf{x} - \mathbf{x}'}{x_G} \right) \delta(z - z'). \tag{2.15}$$

In order to match with Eq. (2.9), we require

$$R(\mathbf{x}) = \frac{E_G^2}{z_G} f\left(\frac{\mathbf{x}}{x_G} \right). \tag{2.16}$$

For power-counting purposes, it is useful to take the limit $f(\boldsymbol{\chi}) \to \delta^{(d-1)}(\boldsymbol{\chi})$, leading to

$$R(\mathbf{x}) \to \sigma^2 \delta^{(d-1)}(\mathbf{x}), \tag{2.17}$$

where, in terms of small-scale parameters,

$$\sigma^2 = \rho_P E_P^2 R^{2(d-1)}. \tag{2.18}$$

Note that all the temperature dependencies from coarse graining disappear in the expression for σ^2. This will be important in Sec. III.

At low temperatures, thermal fluctuations no longer dominate within each Gaussian volume. Instead, the FL conformation is determined by the impurities themselves. To understand how this comes about, consider a segment of FL pinned by two impurities at zero temperature. The elastic energy to deform the segment of length z_G a transverse distance x_G must be compensated by the pinning energy,

$$\tilde{\epsilon}_1 x_G^2 / z_G \sim E_P. \tag{2.19}$$

A comparison of Eq. (2.11) with its low-temperature counterpart Eq. (2.19) shows them to be identical up to the replacement $T \to E_P$. Thus

$$z_G \sim \rho_P^{-\frac{2}{d+1}} \left(\frac{\tilde{\epsilon}_1}{E_P} \right)^{\frac{d-1}{d+1}}, \tag{2.20}$$

with x_G given by Eq. (2.19). Since there are also no

thermal fluctuations, Eq. (2.13) is replaced by $E_G \sim E_P$. Equation (2.16) remains valid, while similar reasoning leads to

$$\sigma^2 = \left[\frac{E_P^{4d}\rho_P^{3-d}}{\tilde{\epsilon}_1^{2(d-1)}}\right]^{1/d+1} . \tag{2.21}$$

For $d = 3$, this gives $\sigma^2 = E_P^3/\tilde{\epsilon}_1$.

III. PHASES AND STABILITY

A great deal is known about the behavior of a single vortex line when only one type of defect is present. Even in this case, there is a competition between impurity pinning and thermal fluctuations. When only the extended defect is present, the analysis becomes particularly simple. For a strong defect, or at low temperatures, it is clear that the FL will be localized near the pin, since the free energy of the delocalized state is purely entropic, and therefore can always be made larger than that of the localized state by decreasing T or increasing the pinning strength. A variety of methods[7,20,21] show that, for $d - n \leq 2$, the FL is localized by an arbitrarily weak extended defect, while for $d - n > 2$, a finite pinning strength is required to "freeze" the FL into a localized state. In three dimensions, the only possible phase in the absence of point impurities is therefore the localized one. Since the defect energy is dominant, this is an ordered phase, described in the renormalization-group (RG) language by a zero-temperature fixed point (sink).

An important quantity is the localization length $\ell_\perp$ within which the FL is confined to the defect. It may be defined by

$$\ell_\perp \equiv \langle |\mathbf{x}(z)|^2 \rangle^{1/2}, \tag{3.1}$$

where the angular brackets denote a thermal average. For the columnar defect ($n = 1$) in three dimensions, the criterion for localization at high temperatures is only marginally satisfied (i.e., $d - n = 2$). As pointed out in Ref. 7, this implies that the localization length is a rapidly increasing function of temperature,

$$\ell_\perp(T) \sim b_0 e^{(T/T^*)^2}, \tag{3.2}$$

where $T^* \equiv \sqrt{\tilde{\epsilon}_1 U_0} b_0$ characterizes the strength of the columnar pin. Since $\ell_\perp$ is such a rapidly growing function of T, one must be careful in applying the single-FL treatment of this paper to situations where $\ell_\perp$ exceeds other relevant scales of the problem, such as the intervortex or interdefect separation. The corresponding length for the planar defect grows much more slowly, as

$$\ell_\perp(T) \sim b_0 (T/T_{\rm pl})^2, \tag{3.3}$$

where $T_{\rm pl} = \sqrt{U_0 b_0 \tilde{\epsilon}_1}$.

When only bulk impurities are present, the problem is much more difficult, but is also now well understood due to extensive numerical and theoretical work.[11–13] Just as in the previous case, while at low temperatures the FL is pinned, it may be depinned at higher temperatures in dimensions greater than 3. Thus, in the dimensions of interest, only a single phase is possible, described by a (different) zero-temperature fixed point. In fact, this phase is the zero-density limit of the proposed vortex glass.[3] To contrast with the localized phase described above, we will denote this the delocalized phase. Care should be taken not to confuse this delocalized phase with the thermally depinned (and also unconfined) phase possible in higher dimensions.

Several properties will be important in what follows. Although the randomness is dominant, the free energy per unit length is self-averaging and approaches a constant, $F(L)/L \to \overline{F(L)}/L \equiv -F_0$. Fluctuations in free energy and transverse extension also grow with length (albeit more slowly), and are described by nontrivial power laws

$$\delta F \sim A L^\omega \quad \text{and} \quad \delta x \sim B L^\zeta, \tag{3.4}$$

where for short-range correlated disorder, the exponents ω and ζ depend only on d and obey $\omega = 2\zeta - 1$.[23,22] The exponent ζ is exactly $2/3$ in $d = 2$, approximately 0.61 in $d = 3$, and gradually reduces to $1/2$ in higher dimensions.[12] Once again, because three dimensions is a marginal case, there is a long length scale at high temperatures before this asymptotic behavior dominates. The randomness of V_P in the z direction causes this length scale, $w(T)$, to grow more rapidly with temperature than $\ell_\perp(T)$ in the previous case,[24]

$$w(T) \sim w_0 e^{(T/T_p)^3}, \tag{3.5}$$

where $T_p = (\tilde{\epsilon}_1 \sigma^2)^{1/3}$ is a characteristic temperature and $w_0 \sim x_G \sim (T/\tilde{\epsilon}_1 \rho_P)^{1/4}$ is the cutoff width [cf. Eq. (2.12)]. Thus, at high temperatures, one expects the effects of the extended defect to dominate experimentally.

To determine whether these phases persist in the presence of *both* an extended defect *and* bulk randomness, we determine their stability to weak perturbations of the complementary interactions. Because the fixed points are at zero temperature, it is sufficient to consider the stability in the absence of thermal fluctuations. The problem of calculating the partition function reduces to that of finding the optimal path for the FL. Correspondingly, the free energy can be reduced to simply the energy.

It is straightforward to show the stability of the localized phase to weak point randomness. In order to destabilize the localized state, the FL would need to achieve a lower energy in a delocalized conformation. However, the optimal energy in the delocalized configuration (at zero temperature) is self-averaging, and, in the limit of weak disorder, much less favorable than that of the localized state. To improve its energy, the FL would need to return to the defect a number of times proportional to its length—i.e., it would be localized, a contradiction. In fact, small regions of the FL will pull away from the defect to take advantage of local energy fluctuations, increasing the localization length (though keeping it finite). There are now, of course, sample-to-sample fluctuations of the energy (or free energy). In this weak-disorder limit, these result from the addition of random energies from each of

the regions of width $\ell_\perp$. Adding up these contributions gives a scaling

$$\delta E \sim AL^{1/2} \quad \text{(columnar defect)}, \tag{3.6}$$

which we expect to be valid throughout the localized phase by continuity (i.e., so long as the fluctuating regions remain finite). For higher-dimensional defects, the contributions for each such region are no longer independent. Since they can be optimized within the defect, they instead lead to a smaller power law,

$$\delta E \sim AL^{\omega_n}, \tag{3.7}$$

where ω_n is the energy exponent for a FL interacting with point defects in n dimensions.

The stability of the delocalized phase is much more difficult to ascertain. This difference occurs because, while there is no way for the FL to be "weakly" delocalized, it certainly can be weakly localized. Such an instability of the delocalized phase corresponds to the formation of a localized state for any nonzero strength of the extended defect; the localization length goes continuously to infinity as the defect strength goes to zero. To investigate this possibility, consider the energy of such a weakly localized FL. The localization length is estimated by minimizing the FL energy

$$E(L,\ell_\perp) = -U_0 L/\ell_\perp^{d-n} + AL/\ell_\perp^{\frac{1-\omega}{\zeta}} - E_0 L. \tag{3.8}$$

The first term is the attractive contribution from the defect, while the second term uses Eq. (3.4) to account for the energy cost of confining the FL into $L/\ell_\perp^{1/\zeta}$ regions of length $\ell_\perp^{1/\zeta}$ and width $\ell_\perp$ (see Fig. 2).[25] Whether or not the pinning term is dominant at large distances determines its relevance. A weak potential is irrelevant for $d > d_l$, where d_l is the *lower critical dimension*, defined by

$$(d_l - n)\zeta = 1 - \omega. \tag{3.9}$$

Using the above estimates of ζ, $d_l = 2$ for columnar defects ($n = 1$), while $3 < d_l < 4$ for planar defects ($n = 2$). A single flux line in three dimensions is thus always pinned by a planar defect. When weak pinning is relevant, minimizing Eq. (3.8) yields a localization length that diverges for small U_0 as

$$\ell_\perp \sim U_0^{-\nu_\perp^0}, \quad \text{where} \quad \nu_\perp^0 = \frac{\zeta}{1-\omega-(d-n)\zeta}. \tag{3.10}$$

For the planar defect, $\nu_\perp^0 \approx 3.6$.

These results can be put on a more formal footing by appealing to the RG. In this picture, the stability of the delocalized phase is determined by the relevance of V_D. At the delocalized fixed point, position and temperature rescale as

$$z \to bz, \tag{3.11}$$

$$\mathbf{x} \to b^\zeta \mathbf{x}, \tag{3.12}$$

$$T \to b^\omega T. \tag{3.13}$$

For this purpose, the defect potential may be approximated by a $(d-n)$-dimensional δ function, which leads to the result

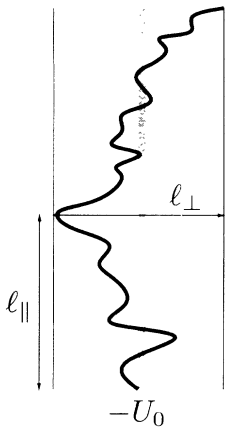

FIG. 2. Schematic illustration of a weakly localized FL. Between regions of width $\ell_\perp$ and height $\ell_\parallel$, the FL must pay an energy cost ($\sim \ell_\perp^{\omega/\zeta}$) to remain localized. This cost is balanced by the loss of energy from the weak defect ($\sim U_0\ell_\parallel/\ell_\perp^{d-n}$).

$$V_D \to b^{1-\omega-(d-n)\zeta} V_D = b^{2-2\zeta-(d-n)\zeta} V_D, \tag{3.14}$$

which is equivalent to the criterion of Eq. (3.9).

This reformulation suggests that a RG expansion in powers of V_D might be systematically made for d near d_l. Defining $V_D(\mathbf{x}) = \Delta f(\mathbf{x})$, with $f(\mathbf{x})$ a short-range function of $\mathbf{x}$ of order 1, Eq. (3.14) becomes

$$\left.\frac{d\Delta}{dl}\right|_{\text{SC}} = -\epsilon\zeta\Delta, \tag{3.15}$$

where $\epsilon = d - d_l$ and the label "SC" indicates that only the explicit scale changes have been included. To convert this into an ϵ expansion, the effects of fluctuations or higher-order terms in V_D must be included. The natural expectation is that these corrections will yield an equation of the form[26]

$$\frac{d\Delta}{dl} = -\epsilon\zeta\Delta + c\Delta^2 + O(\Delta^3), \tag{3.16}$$

where c is a (cutoff-dependent) constant. Equation (3.16) makes two main assumptions. First, the linear term must be unaffected by fluctuation effects. In most renormalization-group calculations this holds true. A notable exception is the case of the sine-Gordon or roughening model. Unlike the roughening model, however, the fields in the FL problem are not dimensionless, so this is not expected to be a problem. Second, the quadratic term is assumed not to vanish and occur with positive sign. Generically, one expects a second-order term to exist, but the sign is not *a priori* clear.

In fact, the sign of this term is crucial to the existence of a well-behaved RG for the delocalization transition. If positive, a fixed point occurs at weak coupling,

$$\Delta^* = \epsilon\zeta/c + O(\epsilon^2). \tag{3.17}$$

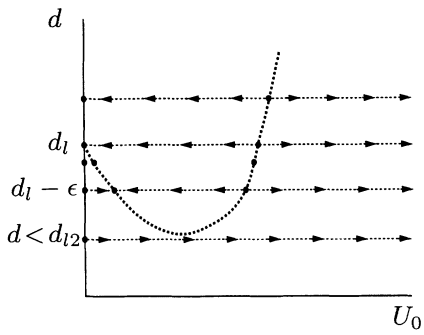

FIG. 3. Dimension-phase diagram for a hypothetical RG scheme with a negative quadratic term. At the lower critical dimension, there is an unbinding transition with nonzero Δ_c. For $d < d_l$, the delocalized fixed point bifurcates, creating a *stable* fixed point at $O(\epsilon)$. The simple delocalized phase is thus replaced by another scale-invariant state in which both the point randomness and extended defect are important. At higher defect strengths, there is still a transition to a conventional localized phase. Below some other critical dimension, $d < d_{l2}$, the new fixed point could annihilate with the critical fixed point, and only the localized phase would persist. Since d_{l2} is unknown, the crucial test of such a scenario is the presence or absence of a transition for $d = d_l$.

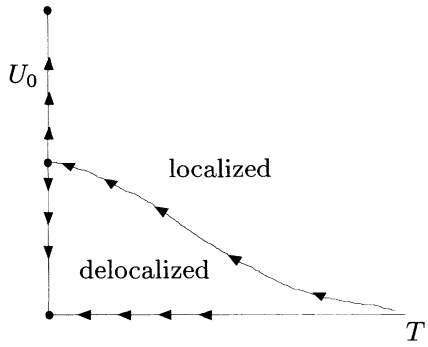

FIG. 4. Schematic RG flows at fixed V_P in the T-V_D plane. There must be at least one critical fixed point, located on the line $T = 0$. The simplest scenario is shown here, with a critical line separating localized and delocalized phases, along which the RG flows lead into the critical point. Because at high temperatures point disorder is more strongly suppressed than the extended defect [cf. Eqs. (3.2) and (3.5)], we expect the phase boundary to approach the $V_D = 0$ axis at high temperatures.

Linearizing around this fixed point, one obtains the universal eigenvalue $\lambda_\Delta = \epsilon\zeta$, which leads to

$$\nu_\perp = \zeta\nu_\parallel = 1/\epsilon + O(1). \tag{3.18}$$

Interestingly, the lowest-order result is independent of c. Had the sign been negative, however, no fixed point would have been found. In fact, such a negative sign leads to a stable fixed point for $d < d_l$, implying a scale-invariant *phase* at intermediate defect strengths, and, presumably, a transition to a true localized state at larger Δ (see Fig. 3). Precisely at the critical dimension, a negative quadratic term implies a delocalization transition at finite Δ.

The computation of even the sign of the quadratic term is extremely nontrivial. To calculate c, it is necessary to know certain properties of the three-point correlation function of V_D at the delocalized fixed point. Unfortunately, the delocalized fixed point itself is nonperturbative for any dimension d (these properties may be determinable in two dimensions using fluctuation-dissipation methods, a possibility currently under investigation[27]). We will return to this question in Sec. VI.

IV. PHASE TRANSITION AND FLORY THEORY

The results of the previous section make clear that in three dimensions there must be an unbinding transition from a columnar pin at an intermediate defect strength. Because both phases are "ordered," one also expects the critical fixed point to be at zero temperature (see Fig. 4 for a schematic RG diagram). Thus, as for the stability analysis, the critical behavior should be describable in terms of optimal paths.

What will be the properties of such a transition? Assuming second-order behavior, one expects the localization length to diverge as the transition is approached from the localized phase. From the size of typical "bubbles," or excursions from the defect, two correlation length exponents $\nu_\perp$ and $\nu_\parallel$ may be defined,

$$\ell_\perp \sim \theta^{-\nu_\perp}, \tag{4.1}$$

$$\ell_\parallel \sim \theta^{-\nu_\parallel}, \tag{4.2}$$

where $\ell_\perp$ is in fact the localization length defined earlier and $\theta \equiv (V_D - V_D^c)$ is the reduced defect strength. From the two correlation lengths, it is natural to define a critical roughness exponent $\zeta_c = \nu_\perp/\nu_\parallel$. A number of arguments indicate that $\zeta_c = \zeta$, the roughness exponent in the bulk, analogously to the behavior at wetting transitions.[20,28] There will also be singularities in the (free) energy, where one conventionally defines the specific heat exponent α by

$$[\langle E_s(L,\theta)\rangle + E_0 L]/L \sim \theta^{2-\alpha}, \tag{4.3}$$

where E_s is the singular part of the FL energy, and E_0 is the energy per unit length of a FL in the bulk.

A simple first attempt at determining these critical exponents is a "Flory"-type argument. Physically, the transition occurs because of the two different ways of resolving the competition between the FL's remaining on the defect and wandering off to take advantage of favorable regions of point pins. Consider a FL very near the transition point on the localized side. Such a line makes large excursions away from the defect, forming "bubbles" of typical size $\ell_\parallel$ and $\ell_\perp \sim \ell_\parallel^\zeta$ in the longitudinal and transverse directions (see Fig. 1). For large $\ell_\parallel$, the energy of a single bubble relative to a pinned segment is

$$\mathcal{E}(\ell_\parallel) = (U_0 - E_0)\ell_\parallel - E_G(\ell_\parallel/a)^\omega. \quad (4.4)$$

The first term is the energy cost (per unit length) of leaving the defect to wander in the bulk; the second term is a typical excess energy gain available (at scale $\ell_\parallel$) due to a favorable arrangement of impurities. Minimizing this energy gives

$$\nu_\parallel^F = 1/(1-\omega), \text{ and } \nu_\perp^F = \zeta/(1-\omega). \quad (4.5)$$

Assuming that the probability of encountering a favorable bubble is independent of its length $\ell_\parallel$, the total number of favorable bubbles is proportional to $L/\ell_\parallel$. The singular part of the FL energy thus scales as

$$E_s(L) \propto \frac{L}{\ell_\parallel}\mathcal{E}(\ell_\parallel) \sim -\theta L. \quad (4.6)$$

The corresponding heat capacity exponent, $\alpha^F = 1$, satisfies a modified hyperscaling form, $2-\alpha = (1-\omega)\nu_\parallel$, appropriate to a zero-temperature fixed point. Application of Eq. (4.5) then gives $\nu_\perp \approx 0.78$, using the numerical values for ζ and ω in $d = 3$.[12]

This Flory-like treatment makes several approximations. First, all bubbles are treated independently, neglecting possible correlations along the FL. Secondly, the energy of each bubble is estimated from the bulk result. This scaling may break down if the constraint of not crossing the defect (necessary to define the bubble consistently) becomes restrictive. A naive estimate of this effect compares the number of returns to the origin of a bulk FL to its energy fluctuations. Such comparison suggests that this effect is unimportant for $d > d_l$, but this treatment is probably too simplistic. Lastly, and possibly most significantly, Eq. (4.4) compares energies only at the largest and smallest scales. In reality, the energy of the FL should be minimized over conformations at *all* length scales.

V. MIGDAL-KADANOFF RENORMALIZATION GROUP

To improve upon the simple approximation of the last section, consider a FL of length $\ell_\parallel$ with both ends fixed at $\mathbf{x} = \mathbf{0}$. Its optimal configuration may be a single pinned segment, a single bubble, or a combination of several bubbles and pinned segments. If the optimal bubble size is to be $\ell_\parallel$, the energies of all the other configurations must be more than that of the single bubble. To ensure this, the energy of the FL must be minimized on all length scales.

This intuitive picture can be made precise by introducing the Berker hierarchical lattice.[29,26] This is a self-similar lattice, constructed iteratively in such a way that the position-space RG can be carried out exactly (see Fig. 5). It can be thought of as the result of the Migdal-Kadanoff "bond-moving" procedure applied to a Euclidean lattice. At every stage in the construction of the lattice, each bond is replaced by q branches of two bonds each. This process leads to the relation $N \propto L^d$, where N is the number of bonds, L is the length of the lattice, and $q = 2^{d-1}$ defines the effective dimensionality d.

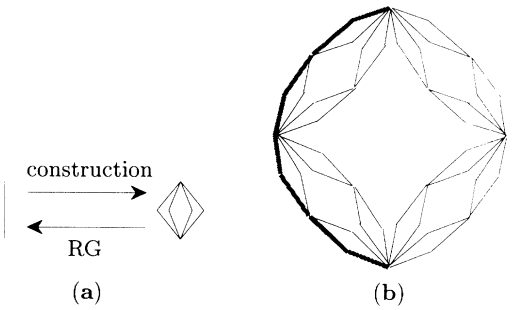

FIG. 5. Berker hierarchical lattice used in Sec. V. Each segment is replaced at the next stage of construction by a set of $q = 2^{d-1}$ branches, as in (a). The resulting lattice after three iterations for the case $q = 2$ is shown in (b). Extended defects can be included by adding an additional binding energy to certain bonds of the lattice. For columnar pins ($n = 1$), these bonds form a single branch spanning the length of the system, indicated here by the thick gray line. The generalization to $n > 1$ is described in Sec. V. To perform the RG, each unit cell of $2q$ bonds is replaced by a single segment, reversing the construction procedure.

To perform the RG transformation, the q branches of the unit cell (see Fig. 5) are collapsed to one, according to

$$E' = \min\{E_1 + E_2, E_3 + E_4, \ldots, E_{2q-1} + E_{2q}\}, \quad (5.1)$$

where E_i is the energy of the ith segment. To treat the defect, certain bonds begin the RG with lower energies. At the first step of the lattice construction, we choose 2^{n-1} of the branches to have such favorable bonds. At each subsequent stage, bulk bonds are replaced by the usual q bulk branches, while defect bonds are again replaced by 2^{n-1} favorable branches and $q - 2^{n-1}$ bulk branches. This construction generalizes the one used in Ref. 26 for columnar pins to other extended defects.

Specializing to the case of the columnar pin ($n = 1$), the defect bonds lie on a single branch of the lattice. Under the RG, the random energies in the bulk induce randomness in the energies on the defect as well. Equation (5.1) can be used to derive the elimination portion of the recursion relations for $p^D(E)$ and $p^B(E)$, the probability distributions of energies on the defect and in the bulk, respectively,

$$\tilde{p}^D_{n+1}(E) = -\frac{d}{dE}\left\{\left[\int_E^\infty dE' \phi^B_n(E')\right]^{q-1}\int_E^\infty dE' \phi^D_n(E')\right\}, \quad (5.2)$$

$$\tilde{p}^B_{n+1}(E) = -\frac{d}{dE}\left\{\left[\int_E^\infty dE' \phi^B_n(E')\right]^{q}\right\}. \quad (5.3)$$

Here n indexes the iteration of the RG, and $\phi^{D,B}(E)$ are the energy distribution functions for pairs of bonds in series, on the defect and in the bulk, respectively. They are given in terms of the single-bond distributions by

$$\phi^{D,B}_n(E) \equiv \int_{-\infty}^\infty dE'\, p^{D,B}_n(E') p^{D,B}_n(E - E'). \quad (5.4)$$

The full RG equations are obtained from Eqs. (5.2) and (5.3) by allowing for the rescaling of energies. These are

$$p^D_{n+1}(E) = 2^{\omega_D}\tilde{p}^D_{n+1}\left[2^{\omega_D}(E+E^D_0)\right], \tag{5.5}$$

$$p^B_{n+1}(E) = 2^{\omega_B}\tilde{p}^B_{n+1}\left[2^{\omega_B}(E+E^B_0)\right], \tag{5.6}$$

where ω_D, ω_B, E^D_0, and E^B_0 must be adjusted to find fixed distributions.

Equations (5.3) and (5.6) decouple, since they are obtained from the RG away from the defect. These equations have been studied extensively by several authors.[30–32] They describe the behavior of a FL in a medium with random point pins, within the Migdal-Kadanoff approximation. For short-range correlated disorder, only a single fixed point exists (up to dimensional rescalings), which must be found numerically for any given q. One finds $\omega_B \approx 0.30, 0.21, 0.19$ for $q = 2, 3, 4$.

Once a solution $p^B(E)$ is found, it must be inserted into Eq. (5.2), which determines $p^D(E)$. Above the critical dimension, this equation has three fixed points, describing the localized phase, delocalized phase, and critical point. Unlike a Euclidean lattice, the hierarchical lattice has $d_c < 2$.[26] In the localized phase, the defect energy is smaller than the bulk energy, so that (at least at scales $> \ell_\parallel$) the FL always chooses to lie on the defect. This occurs if all defect energies are less than all energies in the bulk. In this case, Eq. (5.1) reduces to a $E' = E_1 + E_2$, with all energies drawn from $p^D(E)$. By the central-limit theorem, this leads to a Gaussian fixed-point distribution for $p^D(E)$, with $\omega_D = 1/2$. This is in agreement with the description of the localized phase in Sec. III and in particular with Eq. (3.6). In the delocalized phase, the FL no longer has any preference to lie on the defect. In this case, any coarse-grained segment on the defect will eventually be dominated by a smaller-scale bubble, so that the energies on the defect no longer differ from those in the bulk. Indeed, the ansatz $p^D(E) = p^B(E)$ trivially solves the RG equations, with $\omega_D = \omega_B$ and $E^D_0 = E^B_0$.

The critical fixed point is described by a nontrivial new solution of the RG equations. Since $p^B(E)$ feeds into Eq. (5.2), however, the scaling parameters for the defect must be identical to those in the bulk, i.e.,

$$\omega_D = \omega_B, \tag{5.7}$$

$$E^D_0 = E^B_0. \tag{5.8}$$

Equation (5.7) is the analog, within this approximation, of the statement in Sec. IV that $\zeta_c = \zeta$. Equation (5.8) says that the mean energy per unit length of the FL is constant throughout the delocalized phase and including the critical point. This is very much in contrast to the usual bulk phase transitions, which exhibit symmetric scaling on both sides of the critical point. Precisely this behavior exists, however, in wetting transitions.[20]

The critical exponent $\nu_\parallel$ is determined by linearizing Eq. (5.2) around the critical fixed point. To do this, the bulk fixed-point distribution p^{B*} was calculated by numerical iteration of Eqs. (5.3), (5.4), and (5.6). Once p^{B*} was known, Eq. (5.2) could also be iterated numerically. We took $p^D_0(E)$ to be a Gaussian distribution with mean Δ and the same width as in the bulk. Δ was tuned to its critical value by explicitly watching the evolution of $p^D_n(E)$ (see Fig. 6).

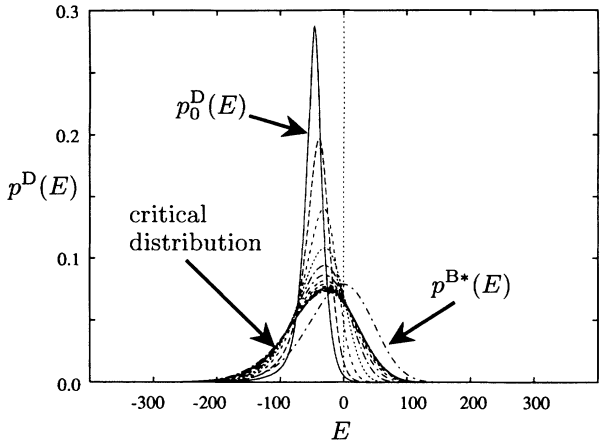

FIG. 6. Determination of the critical fixed-point distribution in the Migdal-Kadanoff approximation. The initial distribution p^D_0 was tuned until it flowed under the RG to the critical point. The bulk fixed-point distribution $p^{B*}(E)$ is also shown, to demonstrate that the critical point has indeed been found.

In principle, linearized versions of Eqs. (5.2), (5.4), and (5.5) may be solved directly to determine the eigenvectors and eigenvalues around the critical point, and hence $\nu_\parallel$. In practice, this would require the discretization of the resulting linear integral equations and the solution of the corresponding matrix eigenvalue problem. To obtain only the largest eigenvalue, an iterative procedure is simpler. We again iterated Eqs. (5.2), (5.4), and (5.5), with $p^D_0(E) = p^{D*}(E+\theta)$. This initial function is decomposable into eigenperturbations δp of the fixed-point form,

$$p^D_0(E) = p^{D*}(E) + \theta\sum_i c_i(\delta p)_i(E), \tag{5.9}$$

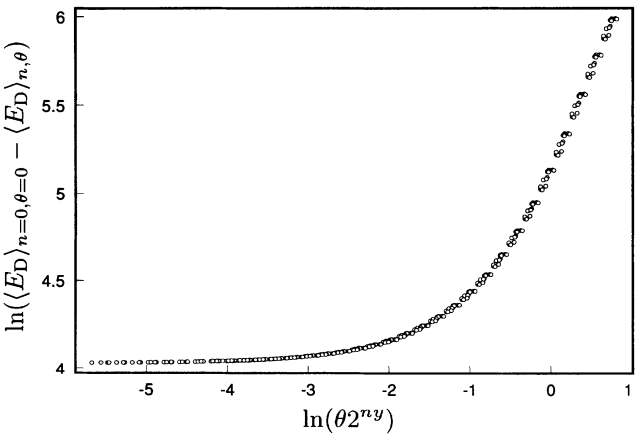

FIG. 7. Scaling collapse of the mean defect energy as a function of length scale and reduced defect strength for $q = 4$ ($d = 3$). Data from 13 systems (different values of θ) fall onto the single universal curve. The eigenvalue $y = 1/\nu_\parallel$, tuned to achieve this collapse, is $y = 0.28$.

TABLE I. Liberation exponents in the Migdal-Kadanoff approximation. The dimension d is defined by the relation $q = 2^{d-1}$. To compute $\nu_\perp$, we used the exponent identity $\omega = 2\zeta - 1$ to define $\zeta = 0.65, 0.61, 0.60$ for $q = 2, 3, 4$ respectively.

q	d	y	$\nu_\parallel$	$\nu_\perp = \zeta\nu_\parallel$
2	2	0.21	4.8	3.1
3	2.6	0.25	4.0	2.4
4	3	0.28	3.6	2.1

where $i = 0$ labels the single relevant eigenfunction and $i > 0$ labels the irrelevant perturbations. Under the RG, c_0 grows according to

$$c_0(n) = c_0(0)2^{ny}, \tag{5.10}$$

where y is the eigenvalue of the perturbation, and is related to the correlation length exponent by $\nu_\parallel = 1/y$. At each step of the iteration, the distribution function defines a mean value

$$\langle E_D\rangle_n \equiv \int_{-\infty}^{\infty} dE\, p_n^D(E)E. \tag{5.11}$$

To determine y, we plotted $\ln(\langle E_D\rangle_{n=0,\theta=0} - \langle E_D\rangle_{n,\theta})$ versus $\ln(\theta 2^{ny})$, for various values of y. Using Eqs. (5.9) and (5.10), this should yield a straight line. In fact, since neither the critical distribution nor $\langle E_D\rangle_{n=0,\theta=0}$ are precisely known, one expects only a scaling collapse. By tuning until such a collapse is found, we determined y and hence $\nu_\parallel$ (see Fig. 7). The results are shown in Table I. For $q = 4$, corresponding to $d = 3$, we find $\nu_\parallel \approx 3.6$. Using the exponent identity to define $\zeta = (1+\omega)/2$, this gives $\nu_\perp \approx 2.1$.

VI. FUNCTIONAL RG AND ϵ EXPANSION

While the approach of the previous section gives a qualitatively appealing picture, the quantitative reliability of the Migdal-Kadanoff approximation is unclear. Ideally, one would like a RG scheme on a Euclidean model, so that the physical dimensionality is taken into account in a controlled way. Because of the nonperturbative nature of the delocalized fixed point for FL's, we introduce a generalized model of a randomly pinned oriented manifold of internal dimension D in the presence of an extended defect. The single internal coordinate z along the FL is replaced by a vector $\mathbf{z} \in \Re^D$, with the transverse coordinate $\mathbf{x}(\mathbf{z}) \in \Re^{N\equiv d-D}$. For example, for $D = 1$, the manifold reduces to a FL, while for $D = d-1$, it may be thought of as an interface. The full free energy is

$$F = \int d^D\mathbf{z}\left\{\tfrac{1}{2}|\nabla\mathbf{x}|^2 - V_P(\mathbf{x}(\mathbf{z}),\mathbf{z}) - V_D(\mathbf{x}_\perp(\mathbf{z}))\right\}, \tag{6.1}$$

where $\mathbf{x}_\perp(\mathbf{z}) \in \Re^{d-n}$, and we have rescaled $\tilde{\epsilon}_1 \to 1$ to avoid confusion with $\epsilon = d - d_l$. We consider only the case $n \geq D$.

The advantage of the generalized model is that, when D is near 4, the zero-temperature fixed point becomes perturbatively accessible.[33] To approach the FL limit of $D = 1$, it is necessary to make a *double* expansion in $\epsilon = d - d_l$ and $\delta = 4 - D$. However, only the sign of the quadratic term in $\partial V_D/\partial l$ matters, and this is probably reliably obtained despite the double expansion.

The delocalized fixed point ($V_D = 0$) was investigated in detail in Ref. 33. For $D = 4 - \delta$, the roughness exponent ζ was found to be proportional to δ. Because $\zeta = O(\delta)$ and $T = 0$, it was necessary to perform a functional RG for the correlation function, $R(\mathbf{x})$, of the point disorder,

$$\langle V_P(\mathbf{x},\mathbf{z})V_P(\mathbf{x}',\mathbf{z}')\rangle \equiv R(\mathbf{x}-\mathbf{x}')\delta(\mathbf{z}-\mathbf{z}'). \tag{6.2}$$

The resulting functional RG equation, valid to lowest order in δ, is

$$\frac{\partial R(\mathbf{x})}{\partial l} = (4 - D - 4\zeta)R(\mathbf{x}) + \zeta x^i\partial_i R(\mathbf{x}) + K_4\left[\tfrac{1}{2}\partial_i\partial_j R(\mathbf{x})\partial_i\partial_j R(\mathbf{x}) - \partial_i\partial_j R(\mathbf{x})\partial_i\partial_j R(\mathbf{0})\right], \tag{6.3}$$

where $\partial_i \equiv \partial/\partial x^i$, and $K_4 = S_4/(2\pi)^4 = 1/(8\pi)^2$. The condition that this equation has a fixed-point solution with $R(\mathbf{x})$ decaying rapidly at large argument (for short-range correlated disorder) determines ζ. To lowest order in δ, the roughness exponent is given by

$$\zeta = \Upsilon\delta + O(\delta^{3/2}), \tag{6.4}$$

where the constant $\Upsilon \approx 1/(4+N)$ (we keep N as an independent variable—i.e., it need not be expanded in δ). With this value for ζ, the fixed-point function is $R^* = O(\delta)$.

To include the effects of the extended defect, the potential $V_D(\mathbf{x}_\perp(\mathbf{z}))$ must be included. In the absence of the random potential, no renormalization of V_D occurs at zero temperature. This is because the optimal configuration of the manifold occurs exactly at the minimum of V_D, since no pins or thermal fluctuations can pull it away. Thus terms of $O(V_D)$ and $O(V_D^2)$ will not contribute in the RG expansion, making all corrections to V_D at least $O(\delta)$.

Formally, the recursion relation for V_D can be derived using the methods of Ref. 33. The relevant diagrams are summarized in Fig. 8. As discussed in the previous paragraph, diagrams containing only V_D vertices vanish at zero temperature [Fig. 8(a)]. To $O(\delta)$, nonvanishing contributions are obtained from graphs with a single disorder vertex [Fig. 8(b)]. The resulting RG equation to $O(RV_D^2)$ is

$$\frac{\partial V_D}{\partial l} = (2 - 2\zeta)V_D + \zeta x^i\partial_i V_D + \frac{K_D}{2}\Lambda^{D-4}\Gamma\nabla^2 V_D + \frac{K_D}{2}\Lambda^{D-6}\Gamma\partial_i\partial_j V_D\partial_i\partial_j V_D, \tag{6.5}$$

where

$$\Gamma \equiv \frac{\langle\nabla V_P(\mathbf{x},\mathbf{z})\cdot\nabla V_P(\mathbf{x},\mathbf{z})\rangle}{N(2\pi)^D\delta^{(D)}(\mathbf{0})} = -\nabla^2 R(\mathbf{0})/N \tag{6.6}$$

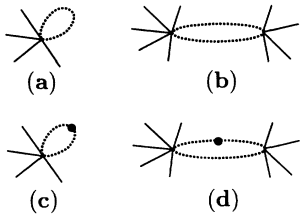

FIG. 8. Diagrams arising in the functional RG treatment of the defect potential V_D. The graphs in (a) and (b) vanish at zero temperature, because they do not involve the bulk randomness. The black circles in (c) and (d) are disorder vertices, which, since V_D is nonrandom, contribute only a factor of Γ.

is positive and $O(\delta)$ at the fixed point. To extract the lower critical dimension, the linearized RG equation must be analyzed in detail. Such an analysis was performed in Ref. 34 for a very similar problem. Denoting $A \equiv K_D \Lambda^{D-4}\Gamma$, the ansatz

$$V_D(\mathbf{x}_\perp) = Q(\mathbf{x}_\perp)\exp\left(-\frac{1}{2}\frac{\zeta}{A}x_\perp^2\right) \tag{6.7}$$

simplifies the linear part of Eq. (6.5) to

$$\frac{\partial Q}{\partial l} = \left(2 - 2\zeta - \frac{N_\perp \zeta}{2}\right)Q - \frac{\zeta^2}{2A}x_\perp^2 Q + \frac{A}{2}\nabla_\perp^2 Q, \tag{6.8}$$

where $N_\perp = d - n$. Letting $Q(\mathbf{x}_\perp, l) = Q(\mathbf{x}_\perp)\exp(\lambda l)$ results in the eigenvalue equation

$$-\frac{A}{2}\nabla^2 Q + \frac{\zeta^2}{2A}x_\perp^2 Q = \left(2 - 2\zeta - \frac{N_\perp\zeta}{2} - \lambda\right)Q. \tag{6.9}$$

Equation (6.9) has the same form as the Schrödinger equation for an $N_\perp$-dimensional simple harmonic oscillator. The various "states" of the oscillator give the eigenfunctions of the linear operator in the RG. The "ground state" is the most relevant operator (largest λ), with

$$\lambda_0 = 2 - 2\zeta - N_\perp\zeta = D - \omega - (d-n)\zeta = -\zeta\epsilon, \tag{6.10}$$

which reproduces the power-counting result [Eq. (3.14)]. The excited states yield eigenvalues larger by integer multiples of $\zeta \sim \delta$, and are thus irrelevant. It is therefore only necessary to consider the single-parameter RG of Eq. (3.16), with Δ defined by

$$V_{D,1}(\mathbf{x}_\perp) = \Delta\exp\left(-\frac{\zeta}{A}x_\perp^2\right). \tag{6.11}$$

Higher-order corrections in R yield total derivatives of V_D (due to the contractions with R vertices). Such terms, like the $\nabla_\perp^2 V_D$ in Eq. (6.5), only change the form of the fixed-point function, and not the eigenvalue, Eq. (6.10).[35] The quadratic term in V_D, by contrast, will be affected at higher order in R. These corrections will modify the coefficient c of the Δ^2 term beyond $O(\delta)$.

To determine c to leading order, an eigenfunction expansion is inserted into Eq. (6.5). Equation (6.7) implies that the left eigenfunction corresponding to $V_{D,1}$ is a constant, so that c is obtained by simply integrating the last term in Eq. (6.5) over $\mathbf{x}_\perp$. Since this term is manifestly positive, $c > 0$. A straightforward Gaussian integration yields the numerical value

$$c = \left(\frac{\pi}{2}\right)^{N_\perp/2}\left(\frac{\zeta}{A}\right)^{2-N_\perp/2} N_\perp(N_\perp+2)\frac{K_D}{2}\Lambda^{D-6}\Gamma, \tag{6.12}$$

valid to $O(\delta)$.

Naively, it appears that the one-loop diagram in Fig. 8(b) contributes for finite momenta, resulting in a renormalization of temperature and a different roughness exponent $\zeta_c \neq \zeta$ at the critical point. Because the defect potential breaks translational invariance, the terms generated by momentum-dependent graphs take the form

$$F' = \int d^D\mathbf{z} M(\mathbf{x}_\perp(\mathbf{z}))|\nabla\mathbf{x}|^2, \tag{6.13}$$

where $M(\mathbf{x}_\perp)$ is a short-range function [since it comes from $V_D(\mathbf{x}_\perp)$]. Because the linear eigenoperators $V_{D,i}$ are short-range functions and not simple polynomials, however, the momentum-dependent terms must be decomposed similarly, into operators of the form

$$K_i \equiv \int d^D\mathbf{z} V_{D,i}(\mathbf{x}_\perp(\mathbf{z}))|\nabla\mathbf{x}|^2, \tag{6.14}$$

and the simple kinetic term

$$K_0 \equiv \frac{1}{2}\int d^D\mathbf{z}|\nabla\mathbf{x}|^2. \tag{6.15}$$

The set K_i do not mix under the linearized RG including the effects of the disorder. For $i > 0$, all the K_i are strongly irrelevant (with dimension $\lambda_i - 2 + 2\zeta$). Therefore, only the projection of the one-loop diagram onto K_0 can potentially contribute to the temperature renormalization. Since $M(\mathbf{x}_\perp)$ is a short-range function, however, this projection is zero. We believe that this continues to hold to all higher orders, so that $\zeta_c = \zeta$ exactly.

Having established the validity of the ϵ expansion, Eq. (3.18) may be evaluated with confidence. For a FL and a columnar defect in three dimensions,

$$\nu_\perp \approx \frac{\zeta}{(d-n+2)\zeta - 2} = \frac{\zeta}{4\zeta - 2}. \tag{6.16}$$

Using $\zeta = 0.61 \pm 0.01$,[12] we find $\nu_\perp = 1.4 \pm 0.1$.

The RG also determines the singularities in the free energy at the transition, and hence α. Defining

$$f \equiv -T\overline{\ln Z}/L^D, \tag{6.17}$$

the RG yields the inhomogeneous scaling relation

$$f(\Delta,T) = e^{-Dl}\frac{T}{T(l)}f(\Delta(l),T(l)) - \frac{\Gamma\Lambda^D K_D}{2}\int_0^l ds e^{-Ds}\frac{T}{T(s)}, \tag{6.18}$$

where the last term results from the $O(R)$ diagram in Fig. 9, and the first term arises from the scale changes. $\Delta(l)$ and $T(l)$ are determined by Eq. (3.16) and the continuous analog of Eq. (3.13),

$$\frac{dT}{dl} = -\omega T. \tag{6.19}$$

Solving Eq. (6.19), Eq. (6.18) becomes

$$f(\Delta,T) = e^{-(D-\omega)l} f(\Delta(l), Te^{-\omega l}) - \frac{\Gamma\Lambda^D K_D}{2}\int_0^l ds e^{-(D-\omega)s}. \tag{6.20}$$

At low temperatures, entropic contributions become negligible, and $f(\Delta,T) \to u(\Delta)$. Thus

$$u(\Delta) = e^{-(D-\omega)l} u(\Delta(l)) - \frac{\Gamma\Lambda^D K_D}{2}\int_0^l ds\, e^{-(D-\omega)s}. \tag{6.21}$$

On the delocalized side of the transition, $\Delta(l) \to 0$ for large l. In this limit, u goes smoothly to its bulk value E_0. Since $D-\omega = 2(1-\zeta) > 0$, the first term of Eq. (6.21) vanishes and the last term is nonsingular and independent of Δ. In agreement with both the Flory and Migdal-Kadanoff theories, the mean line energy is independent of Δ on the delocalized side of the transition. In an experiment, where the actual tuning parameter is the temperature, the free energy will not, of course, be independent of T in the delocalized phase. It should, however, be free of singular behavior as the transition is approached from this side.

In the localized phase, $\Delta(l)$ becomes large for large l. For large Δ, the FL will be fully localized on the defect, so $u \propto \Delta$. Unlike the delocalized case, the first term in Eq. (6.21) cannot be ignored. To understand its effects near the transition, Eq. (6.21) can be rewritten in terms of the reduced defect strength as

$$u(\theta) = e^{-(D-\omega)l} u(\theta e^{l/\nu_\parallel}) - \frac{\Gamma\Lambda^D K_D}{2}\int_0^l ds e^{-(D-\omega)s}. \tag{6.22}$$

Choosing $e^l = \theta^{-\nu_\parallel} = \ell_\parallel/a$, this becomes

$$u(\theta) = (\ell_\parallel/a)^{-(D-\omega)} u(\theta=1) - \frac{\Gamma\Lambda^D K_D}{2(D-\omega)}\left[1-(\ell_\parallel/a)^{D-\omega}\right]. \tag{6.23}$$

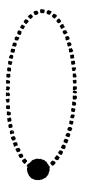

FIG. 9. $O(R)$ diagram renormalizing the free energy. Integrating out this vertex leads to the inhomogeneous term in Eq. (6.17).

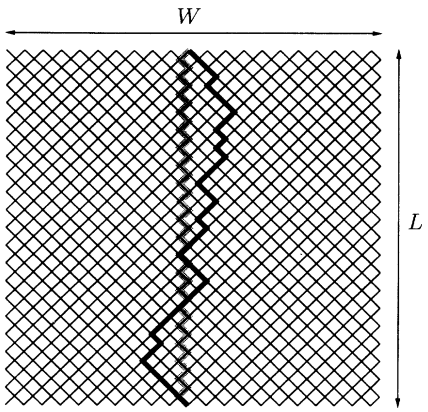

FIG. 10. Flux line directed along the diagonal of a square lattice, as utilized in the simulations of Sec. VII. Random energies were assigned independently to each bond of the lattice, with a fixed defect energy on bonds along a defect (thick gray) at the origin.

The two contributions do not cancel on this side of the transition (as they must according to the previous argument in the delocalized phase), leading to singular behavior with $2-\alpha = (D-\omega)\nu_\parallel$, the appropriate modification of hyperscaling for this zero–temperature fixed point. For the FL and columnar pin in three dimensions, $\alpha \approx 0.21$.

VII. NUMERICAL SIMULATIONS

To check the predictions of Secs. III–VI, we examined the problem numerically at zero temperature by a transfer-matrix method which locates the optimal path exactly in a strip of finite width. To enhance performance, we chose the z direction along the diagonal of a square or cubic lattice, with random energies on the bonds (see Fig. 10). The energies of optimal paths terminating at position $\mathbf{x}$ at height z obey the recursion relation

$$E(\mathbf{x},z+1) = \min_{|\mathbf{x}-\mathbf{x}'|=1}\{E(\mathbf{x}',z) + V_P(\mathbf{x},\mathbf{x}',z) - \Delta\delta(\mathbf{x}_\perp)\}, \tag{7.1}$$

where $V_P(\mathbf{x},\mathbf{x}',z)$ is the random energy assigned to the bond connecting the points $(\mathbf{x},z+1)$ and $(\mathbf{x}',z)$, and $\delta(\mathbf{x}_\perp)$ is an appropriate lattice δ function indicating when the FL is on the defect. Boundary conditions were chosen so that the FL remains within a strip of width W. For simplicity, the random bond energies were drawn from a uniform distribution of integers with mean 0 and width 4096.

It is easy to obtain an upper bound on the critical defect strength Δ_c above which the FL is localized. Suppose $\Delta > E_0$, the (negative) mean energy per unit length in the bulk. If the FL were delocalized, its energy per unit length would take this value, because it would spend negligible time on the defect. Since $\Delta > E_0$, however, the FL can lower its energy simply by remaining on the defect. Therefore the assumption that it is delocalized must

be false, so $\Delta_c \leq E_0$. It is probable that this bound is saturated as $d \to \infty$, but we consider only $d = 2, 3$.

Iteration of Eq. (7.1) yields the optimal paths for a system of width W and length L in a time $T \propto W^{d-1}L$. To calculate quantities defined at a single height z, only two arrays $E(\mathbf{x})$ need to be stored concurrently, requiring memory $M \propto W^{d-1}$. The localization length can be defined as

$$\ell_\perp(W) \equiv \sqrt{\overline{|\langle \mathbf{x} \rangle|^2}}, \tag{7.2}$$

where the angular brackets $\langle \cdots \rangle$ indicate evaluation on the optimal FL, and the overbar, as usual, signifies the disorder average. The mean line energy is simply obtained by averaging the optimal element of the energy array, i.e., $\overline{E_{\min}(\mathbf{x}, L)}/L$. Both the localization length and mean line energy are self-averaging, so that the disorder average may be replaced by an average over z. In the localized phase, segments of the FL of length $\ell_\parallel$ should contribute roughly independently to these z averages. The fractional uncertainty in the average computed in this way should thus scale like $t \sim 1/\sqrt{N} \sim \sqrt{\ell_\parallel/L}$. To avoid large finite-size effects, the width must be chosen to be at least $W \sim a\ell_\perp$, with $a \approx 2$–5. Thus, to obtain good data within a tolerance t in the localized phase requires an execution time of the order

$$\text{time} \sim \frac{a^{d-1}}{t^2} \ell_\perp^{d-1} \ell_\parallel \tag{7.3}$$

time steps. Since both $\ell_\perp$ and $\ell_\parallel$ diverge strongly at the critical point, time limitations become quite important. Using $\nu_\perp = \zeta \nu_\parallel \approx 1.4$, we find $T \sim \theta^{-5.1}$ for the columnar defect in three dimensions. For the planar defect, $\nu_\perp^0 = \zeta \nu_\parallel^0 \approx 3.6$ gives $T \sim \Delta^{-13.2}$.

In addition to these equal-z quantities, it is also interesting to visualize the conformation of the FL in a particular realization of bulk randomness. To compute the optimal configuration of the FL, the transfer-matrix algorithm above must be modified to include nonlocal information. The simplest such modification (though not the most memory efficient) is to store the vertex $\mathbf{x}(z)$ to which the optimal FL terminating at the vertex $\mathbf{x}(z+1)$ is connected, for all $\mathbf{x}(z)$ and all z. The conformations of the FL terminating at any point at $z = L$ can then be constructed by tracing back this connectivity step by step until $z = 0$ (for details of the algorithm, see Ref. 22). Figure 11 shows the configurations for a FL of length $L = 1000$ in two dimensions for four defect strengths. As Δ is increased, the FL collapses more closely to the defect. Such pictures emphasize the presence of bubbles on all scales less than the localization length.

To check the predictions of Sec. III, we studied the behavior of $\ell_\perp(W)$ as a function of W and Δ. Delocalized and localized phases can be distinguished by the behavior of $\ell_\perp(W)$ as a function of W. If the FL is truly delocalized, its transverse fluctuations will be contained only by the strip width, so that $\ell_\perp(W) \sim W$ for large W, independent of Δ. In a localized phase, however, $\ell_\perp(W)$ will settle down to its infinite-system value when $W \gg \ell_\perp(W = \infty)$.

Figure 12(a) shows $\ell_\perp(W)$ versus Δ at several values of W for the columnar defect in three dimensions. We used FL's of length $L \approx 2.5 \times 10^6$ lattice constants with widths up to $W = 250$, and a few larger systems to test the limits of the computer. For $\Delta < 300$, $\ell_\perp(W)$ becomes essentially constant (and $\propto W$) as a function of Δ. The data are in agreement with Sec. III, suggesting an unbinding transition with $\Delta_c \approx 300$. The location of the critical point is reasonable, with $\Delta_c/E_0 \approx 0.2$.

For the planar defect in three dimensions, shown in Fig. 12(b), the behavior for small Δ is quite different. For

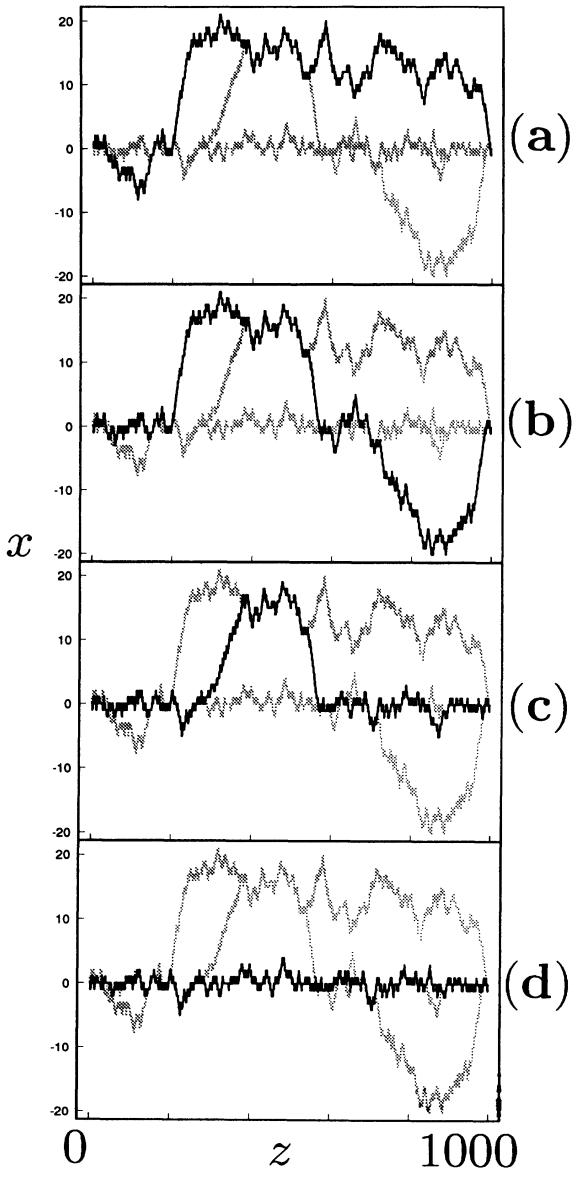

FIG. 11. Optimal conformations of a FL of length $L = 1000$ in two dimensions, with the two ends constrained to lie on the origin. The black curves in (a), (b), (c), (d) show the configurations for $\Delta = 0, 200, 400, 600$, respectively. The other three curves are retained in gray within each frame for comparison. As the defect strength increases, the FL collapses into a more and more compact configuration. Note that "bound" segments actually contain many excursions on scales smaller than the largest bubbles.

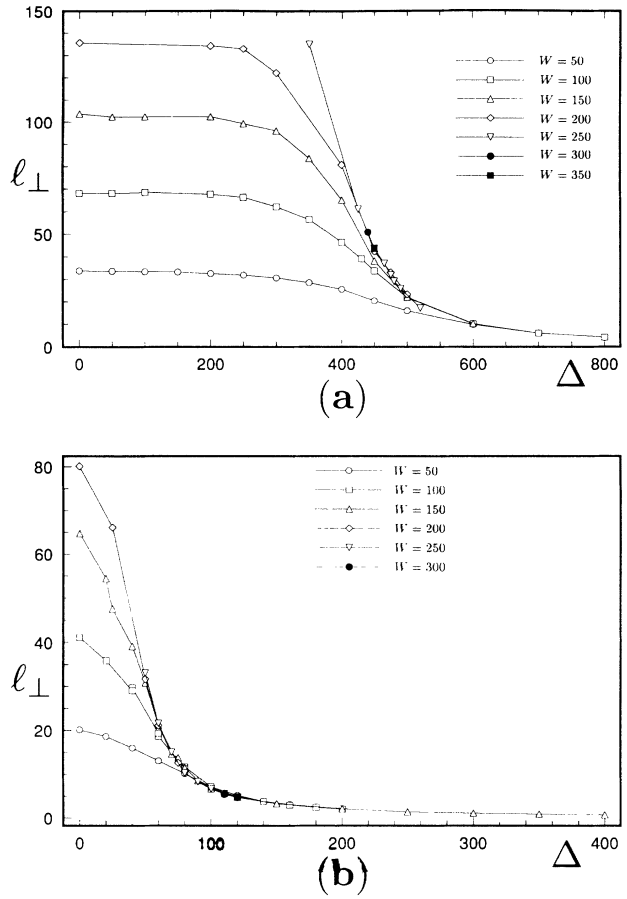

FIG. 12. $\ell_\perp(W)$ as a function of Δ in three dimensions for (a) the columnar defect, and (b) the planar defect. See text for details.

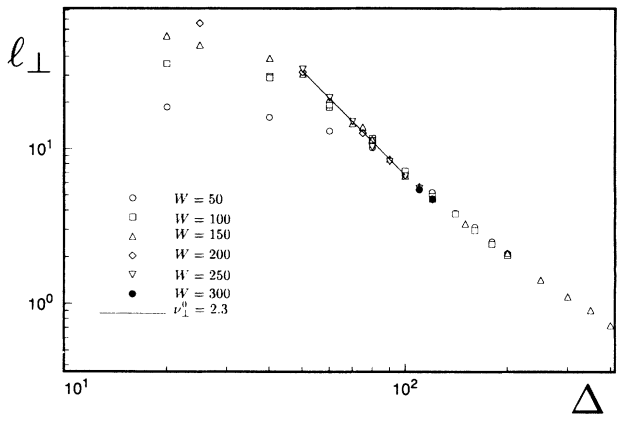

FIG. 13. Log-log plot of the localization length versus defect strength for the planar defect in three dimensions. The line is a least-squares fit to the reliable data for $\Delta \leq 100$. Note the upward curvature, suggesting that the asymptotic power-law behavior has not yet been reached.

$\Delta = 0$, the FL is delocalized, and $\ell_\perp(W) \propto W$. However, within the resolution of the calculation, any nonzero Δ leads to a decrease in $\ell_\perp(W)$. A putative delocalized phase would have to occur for $\Delta_c < 10$. In dimensionless units $\Delta_c/E_0 < 7 \times 10^{-3}$, which strongly suggests that the delocalized phase is in fact absent, in agreement with Sec. III. To check Eq. (3.10), the data are replotted on a log-log scale in Fig. 13. A least-squares linear fit gives $\nu_\perp^0 \approx 2.3$, much less than the predicted value of $\nu_\perp^0 = 3.6$. As noted above [see Eq. (7.3)], the large value of $\nu_\perp^0$ makes finite-size effects particularly strong for the planar defect. A closer examination of Fig. 13 reveals upward curvature, suggesting that a larger value of $\nu_\perp^0$ would be obtained by going to smaller Δ.

We also repeated similar simulations in two dimensions, where somewhat larger system sizes can be handled ($W = 1600$, $L = 1.6 \times 10^7$ lattice constants). These calculations provide a direct check on the prediction of Sec. VI that the quadratic term in the RG is positive. Since $d = 2$ is the critical dimension for columnar defects, a delocalized phase for small Δ can only exist if this term is negative. Figure 14 shows $\ell_\perp(W)$ versus Δ for this case. As for the planar defect in three dimensions, the data put a bound on the dimensionless critical defect strength. Using the measured value $E_0 \approx 1100$, we find $\Delta_c/E_0 < 0.09$. Further support for the RG is obtained by plotting $\ln[\ell_\perp(W)]$ versus $1/\Delta$ (see Fig. 15). The resulting straight line implies $\ell_\perp \sim \ell_{\perp 0} \exp(\Delta^*/\Delta)$, which is the RG prediction in the critical dimension. A least-squares fit gives $\ell_{\perp 0} \approx 0.3$ and $\Delta^* \approx 1000$, in agreement with the lattice length scale and energy scale set by the disorder width. Note that previous numerical investigations in two dimensions for this problem,[36] and for pinning by an attractive wall,[37] both saw an unbinding transition with nonzero Δ_c. While the attractive wall is probably in a different universality class, we believe the earlier study by one of us[36] for this problem was hampered by finite-size effects.

We next turn to the critical point for the columnar pin in three dimensions. The main difficulty in this analysis is in the determination of the critical defect strength Δ_c. To do so, we made log-log plots of $\ell_\perp$ versus $\theta \equiv (\Delta - \Delta_c)/\Delta_c$ for a range of values of Δ_c. The result is shown in Fig. 16. Plausible linear behavior is observed for $300 < \Delta_c < 435$. Least-squares fits to the linear regions give the range of values $\nu_\perp = 1.3 \pm 0.6$. This result is consistent with all three estimates (Flory, Migdal-Kadanoff, and RG), though the best curve in Fig. 16 gives the mean value quite close to the RG estimate, $\nu_\perp \approx 1.4$.

VIII. POSSIBLE EXPERIMENTS AND SIMULATIONS

A. Applicability of the single-flux-line limit

In order to compare the predictions of this paper with experiment we must account for several complications not included in our treatment. Both extended defects and FL's appear at finite densities and their lengths are limited by the sample thickness. First consider a single FL in a random set of columnar pins at zero temperature. The FL can be unpinned from a particular defect by two mechanisms. When the localization length $\ell_\perp$ becomes

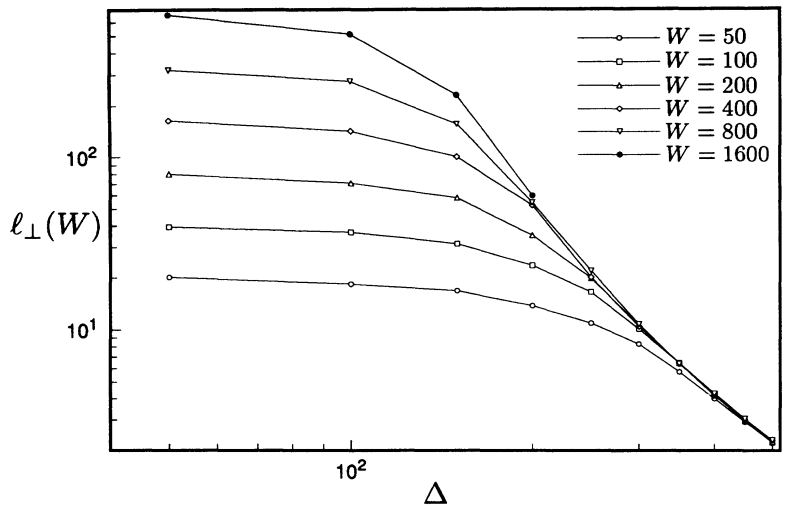

FIG. 14. Localization length $\ell_\perp(W)$ as a function of Δ for the columnar defect in two dimensions. No evidence of a transition is seen. A careful examination of the topmost curve reveals a slight upward curvature, suggesting a non-power-law divergence of $\ell_\perp$ for small Δ.

comparable to the typical defect separation $\bar{\ell}_{\perp,d} \equiv \rho_d^{-1/2}$, the FL can freely wander between pins. (It may still be collectively localized by randomness in the distribution of columnar pins at a much larger length scale.) The second mechanism, originally described in the context of the Bose glass,[9] involves a long-range hopping mechanism in which a FL wanders to a distant pin. The energy cost of such a move is given by a variable-range-hopping argument. Consider a "kink," such as that shown in Fig. 17, in which a segment of FL is cast from the best columnar defect onto another far away pin. The energy of the best such kink of length $L_\parallel$ and width $L_\perp$ is (cf. Ref. 7)

$$\Delta E_{\rm kink} \sim 2\epsilon_0 L_\perp + \frac{L_\parallel}{g(U_0)\rho_d L_\perp^{d-1}}, \tag{8.1}$$

where the energy per length of the far pin is estimated as $U_0 + 1/\left[g(U_0)\rho_d L_\perp^{d-1}\right]$. Here, $g(U_0)$ is the density of states in energy for columnar defects at U_0, and is probably of order of some fraction of $1/U_0$. For a given $L_\parallel$, the optimal kink has an energy

$$\Delta E_{\rm VRH} \sim \epsilon_0 \left[\frac{L_\parallel}{g(U_0)\rho_d \epsilon_0}\right]^{1/d}, \tag{8.2}$$

and a width $L_\perp \sim [L_\parallel/g(U_0)\rho_d\epsilon_0]^{1/d}$. Local fluctuations of point pins can compensate for this energy cost. In the (not too strongly) localized regime of the single-pin problem, energy fluctuations obey a scaling form

$$\Delta E_{\rm pt} \sim E_G \left(\frac{L_\parallel}{a}\right)^\omega h(L_\parallel/\ell_\parallel), \tag{8.3}$$

where $h(\chi)$ is a universal scaling function. In the localized phase, $L_\parallel/\ell_\parallel \gg 1$ for long FL's. For consistency with Eq. (3.6), the large-argument behavior of the scaling function is $h(\chi) \to \chi^{1/2-\omega}$, leading to

$$\Delta E_{\rm pt} \sim E_G \left(\frac{\ell_\parallel}{a}\right)^\omega \left(\frac{L_\parallel}{\ell_\parallel}\right)^{1/2}. \tag{8.4}$$

Equation (8.4) demonstrates that the total energy fluctuations are obtained by summing fluctuations within localization volumes of length $\ell_\parallel$. The scaling argument also agrees with an exact calculation of energy fluctuations of a FL pinned to a wall[36] in two dimensions. When $\ell_\parallel/a \ll 1$, the FL is strongly localized on the columnar pin, and energy fluctuations come only from point pins lying within a distance $R + b_0$ from the defect center. Equation (8.4) is then replaced by

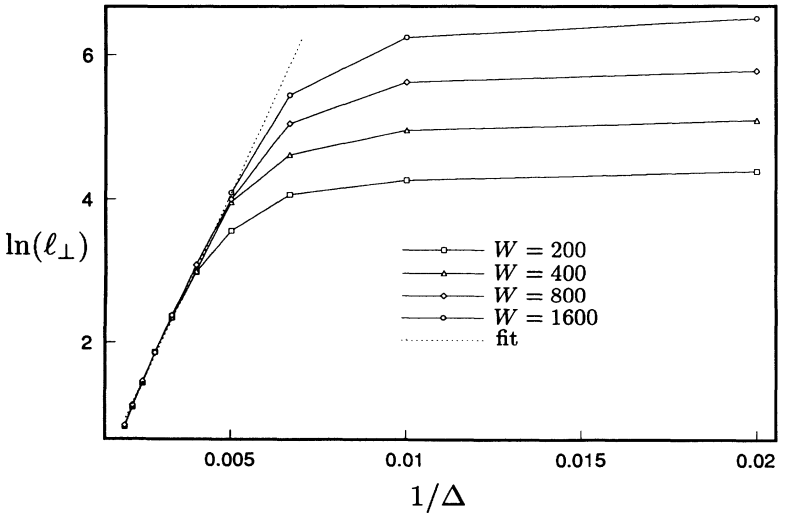

FIG. 15. Plot of $\ln(\ell_\perp)$ versus $1/\Delta$ for the columnar pin in two dimensions. The straight line is a least-squares fit to the exponential form $\ell_\perp \sim \ell_{\perp 0}\exp(\Delta^*/\Delta)$ (see Sec. VII).

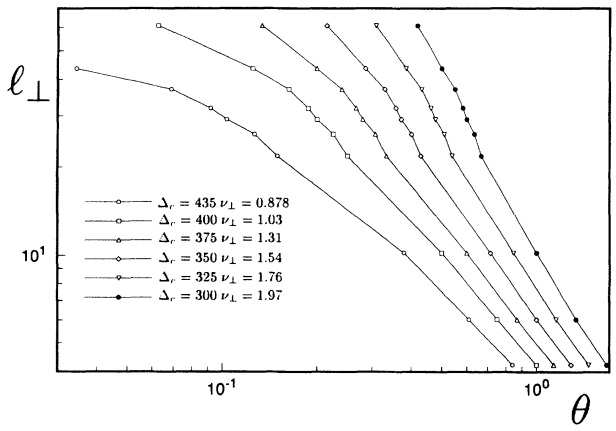

FIG. 16. Log-log plot of the localization length versus $\theta \equiv (\Delta - \Delta_c)/\Delta_c$, for the columnar defect in three dimensions. The different curves represent choices of Δ_c, which is adjusted to achieve the most linear behavior.

$$\Delta E_{\rm pt,SL} \sim E_P \left[\pi(R+b_0)^2 \rho_P L_\parallel\right]^{1/2}. \tag{8.5}$$

A reasonable criterion for the strongly localized regime is $\theta_{\rm MF} \equiv U_0 a/E_G - 1 \gg 1$. Since the kink energy grows more slowly than $L^{1/2}$ for $d > 2$, the FL will become delocalized through quenched-in kink formation for $L > L_{\rm hop}$, where

$$L_{\rm hop} \sim \left[\left(\frac{a}{\ell_\parallel}\right)^\omega \frac{\epsilon_0}{E_G} \frac{\ell_\parallel^{1/2}}{[g(U_0)\rho_d \epsilon_0]^{1/d}}\right]^{\frac{2d}{d-2}}, \tag{8.6}$$

for $\ell_\parallel/a \gg 1$, while in the strongly localized regime

$$L_{\rm hop,SL} \sim \left[\frac{\epsilon_0}{E_P}[g(U_0)\rho_d\epsilon_0]^{-1/d}(\pi[R+b_0]^2\rho_P)^{-1/2}\right]^{\frac{2d}{d-2}}. \tag{8.7}$$

The borderline case of $d = 2$ is more subtle and will not be treated here.[38] The pinning effects described in this paper are thus applicable only for $L \ll L_{\rm hop}$ and $\ell_\perp \ll \bar{\ell}_{\perp,d}$. A finite density of FL's introduces another length scale $\bar{\ell}_{\perp,\rm FL} \equiv \rho_{\rm FL}^{1/d-1}$. The dilute Bose glass for $\bar{\ell}_{\perp,\rm FL} \gg \bar{\ell}_{\perp,d}$ is subject to the same constraints, and is unstable to the above hopping mechanism[9] for $L \gg L_{\rm hop}$. In the overdense limit of $\bar{\ell}_{\perp,\rm FL} \ll \bar{\ell}_{\perp,d}$, the hopping mechanism is no longer relevant. A remnant of the unpinning transition may still be observed for $\ell_\perp \ll \bar{\ell}_{\perp,\rm FL}$. Similar considerations hold for the case of grain boundary pinning.

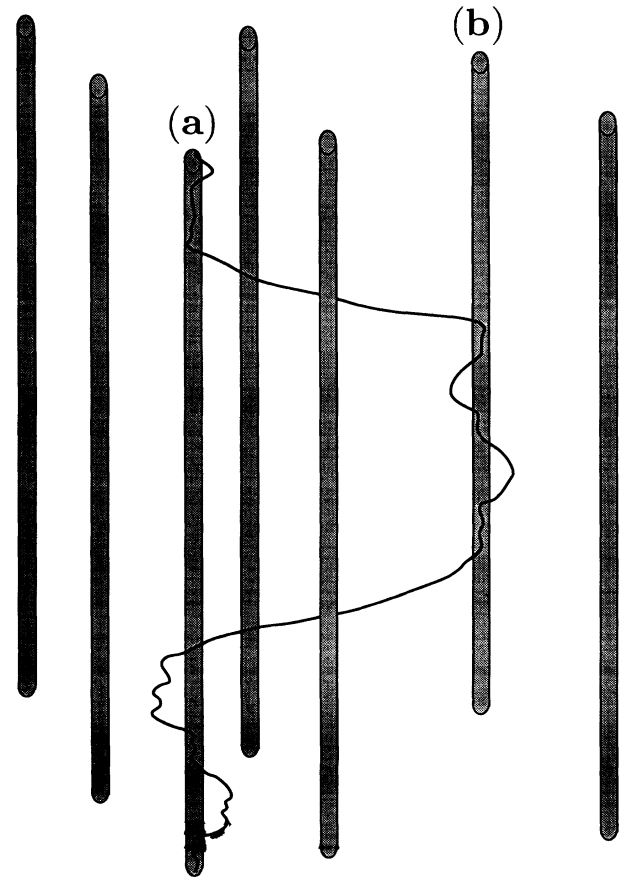

FIG. 17. Single vortex line with many columnar defects. Even though pin (a) has the largest binding energy U_0 energy fluctuations due to point randomness make it favorable for the FL to visit pin (b) by forming a "kink," as shown here.

B. Estimates of physical quantities

Assuming that the above conditions are satisfied, the single-FL model should describe the behavior of the system. As noted in Fig. 4, however, even within this model, a transition only exists for sufficiently strong point pinning. A reasonable criterion for the FL to be delocalized at $T = 0$ is

$$U_0 < E_0 \approx E_G/z_G, \tag{8.8}$$

where E_G and z_G are the low-temperature coarse-graining parameters determined in Sec. IIIIC. To calculate E_0, we need estimates of $\tilde{\epsilon}_1$, E_P, and ρ_P. The FL stiffness constant $\tilde{\epsilon}_1$ is independent of the disorder, and given by Eq. (2.2). For YBCO, the anisotropy factor $\gamma \approx 0.2$. Note that for small-scale distortions, which occur at high impurity concentrations, the FL stiffness is reduced by a factor of γ^2, increasing the effectiveness of point pinning. For YBCO, $\lambda_{ab} \approx 1.4 \times 10^{-5}$ cm, which gives $\epsilon_0 \approx 1.4 \times 10^{-6}$ erg/cm, and, in the small-scale regime,

$$\tilde{\epsilon}_1 \approx 6 \times 10^{-8}\ \text{erg/cm}. \tag{8.9}$$

E_P and ρ_P both depend upon the type of impurity considered. Assuming first oxygen vacancies, a semimicroscopic treatment[19] gives the pinning energy

$$E_G \approx E_P \approx 1.4 \times 10^{-14}\ \text{ergs}. \tag{8.10}$$

Note that this result holds only when the distance between neighboring impurities is larger than ξ_{ab}, i.e., $\rho_P \xi_{ab}^3 \ll 1$. A similar (though slightly smaller) result is obtained from Eq. (2.8), using $r_0 \approx 0.29$ nm, and

including the enhancement factor ξ_{ab}/r_0. A reasonable upper bound on the vacancy density per CuO plane is $n_\square \approx 0.1/\xi_{ab}^2$, above which superconducting properties themselves may be substantially changed. The bulk density is just $\rho_P = n_\square/s$, where s is the spacing between CuO planes. Using $\xi_{ab} \approx 1.5$ nm, and $s \approx 1.2$ nm, we find

$$\rho_P^{\max} \approx 4 \times 10^{19}\ \mathrm{cm}^{-3} \quad \text{(YBCO)}. \tag{8.11}$$

Equation (2.20) then gives $z_G \approx 3$ nm, so

$$E_0 \approx 5 \times 10^{-8}\ \mathrm{erg/cm} \quad \text{(oxygen vacancies)}. \tag{8.12}$$

Precipitates or other mesoscopic inclusions lead to rather different energy and length scales. One candidate is nonsuperconducting regions of Y_2BaCuO_5 in $YBa_2Cu_3O_x$, as have been observed by Murakami *et. al.*[17] in melt-textured samples. Taking characteristic sizes and separations from their Fig. 16, $r_0 \approx 1\ \mu$m and $\rho_P \approx (10\ \mu\mathrm{m})^{-3} \approx 10^9\ \mathrm{cm}^{-3}$. From Eq. (2.6), we find $E_P \approx 4 \times 10^{-9}$ ergs. Using this time the long-distance value for $\tilde{\epsilon}_1$, $z_G \approx 6 \times 10^{-4}$ cm, yielding

$$E_0 \approx 7 \times 10^{-6}\ \mathrm{erg/cm} \quad \text{(precipitates)}. \tag{8.13}$$

It is important to note that the samples of Ref. 17 contained substantial numbers of other defects such as twin and grain boundaries, which are not accounted for in the treatment of this paper. The estimates above are meant as suggestions for possible cleaner samples with large-scale bulk defects.

The line energies in Eqs. (8.12) and (8.13) should be compared with U_0 as obtained from Eq. (2.3). We consider two types of columnar defect: heavy-ion tracks and dislocation lines. Ion tracks are man-made pins created by bombarding a superconducting sample with heavy-ion radiation. Such artificial pinning sites have been created by several groups,[4,5] using a variety of ions. Screw dislocations occur naturally in some samples,[39] depending upon the method of preparation. The radii for these two types of defects can be quite different, with $c_0 \approx 3.0$ nm for Cs ion tracks in Ref. 4, while $c_0 \approx 0.5$–1.0 nm (of order an atomic lattice spacing) is appropriate for a dislocation line.[19] Using these values, Eq. (2.3) gives

$$U_0 \approx \begin{cases} 5 \times 10^{-7}\ \mathrm{erg/cm} & \text{(ion track)}, \\ 4\text{–}20 \times 10^{-8}\ \mathrm{erg/cm} & \text{(dislocation line)}. \end{cases} \tag{8.14}$$

Comparison with Eq. (8.12) shows that oxygen vacancies are probably too weak to delocalize a FL from an ion track, while unpinning from a dislocation line *is* possible. Pinning energies from precipitates, Eq. (8.13), are substantially higher, and may allow for unbinding even from ion tracks. The difficulties in obtaining a sufficiently large, high-quality sample with such large-scale defects are, however, formidable.

C. Suggestions for observation

Based on the results of the previous section, the best candidate for observing FL delocalization is a twin-free crystal containing dislocation lines separated by distances much greater than the penetration depth. Given such a sample, there are several ways in which the localization length of the FL may be probed.

The most direct method is surface imaging of the FL array. Ideally, one would like to map out the displacement of a pinned vortex line as a function of temperature, averaging over many such pinned vortex lines, to obtain $\ell_\perp(T)$. In practice, surface pinning and interactions may make the displacement of the FL end point scale differently than in the interior of the sample. Probably such complications could be dealt with, but further investigation is certainly required. A more serious problem is an experimental limitation of the decoration techniques currently used for such imaging.[40] In these experiments, a magnetic "smoke" is introduced above a sample in a vacuum chamber. The magnetic particles attach themselves preferentially to the regions of flux around the vortex lines, forming an image at the surface. Unfortunately, this deposition is quite slow, and must be performed at low temperatures. The observed flux lattice is thus probably frozen into some metastable pinned state at higher temperatures, selected according to the sample's cooling history. Since the point at which the system freezes is unclear, the temperature of a particular image, as well as the extent to which it has equilibrated, is unknown.

Recently, Harada *et al.*[41] have developed a holographic technique capable of real-time imaging. Once this technology is in place, it will be possible to determine sample temperatures and equilibration times by direct observation. This should allow the experimenters to measure FL displacements directly.

Since these imaging techniques are difficult and cannot probe the interior of the sample, it is useful to look for a signature of the localization length in a bulk measurement. Here, we consider the effects of a nonzero localization length on low-temperature transport measurements. Since the FL is pinned, transport is dominated by thermally activated flux creep, in which the energy barriers to motion lead to nonlinear I-V characteristics. These characteristics have been considered for point disorder in Ref. 3 and for a columnar defect in Ref. 7. In both cases, the creep is dominated by critical excitations, in which a region of FL jumps forward in response to the Lorentz force from the applied current.

In the localized phase at low temperatures, at least naively, two types of excitations are present (see Fig. 18). For very small currents, the Lorentz energy dominates only for very large FL segments and displacements. When this excitation becomes much larger than the localization length, its energetics are dominated by the columnar defect. As the current is increased, excitations may be possible on scales smaller than the localization length. These short FL segments are pinned by point impurities, and thus have a different energy scale for their barriers to motion.

For the large excitations, Ref. 7 gives the barrier energy

$$E_B(L_\parallel \gg \ell_\parallel) \sim U_R \left(\frac{U_R}{\tilde{\epsilon}_1}\right)^{1/2} \frac{c\tilde{\epsilon}_1}{J\phi_0}, \tag{8.15}$$

where we have replaced the bare defect energy U_0 by its

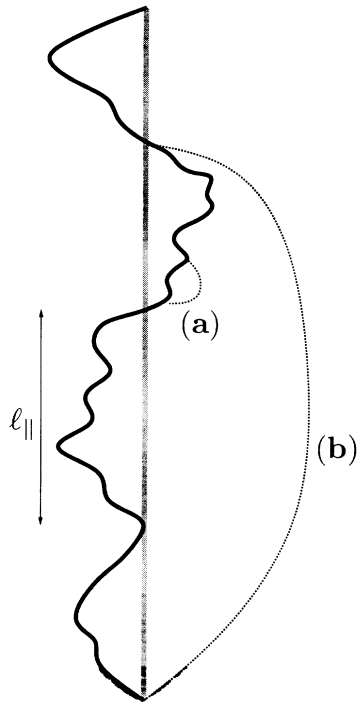

FIG. 18. Two types of critical excitations on a localized FL. For currents smaller than the zero-temperature critical current, a voltage is produced by thermally activated production of vortex loops. When this current is large enough ($J \gg J_{\rm CP}$), small loops, such as (a), unbind at scales much less than the localization length. The energy barriers dominating this process are set by the point disorder. For much lower currents, larger loops, such as (b), control the depinning. When these loops are much larger than the localization length ($J \ll J_{\rm CP}$), the energy barriers are controlled by the renormalized columnar defect strength.

renormalized value U_R in the presence of point defects. It has the limiting behaviors [see Eq. (6.23)]

$$U_R \sim \begin{cases} (a/\ell_\parallel)^{1-\omega} U_c, & \ell_\parallel \gg a, \\ U_0, & \ell_\parallel \lesssim a, \end{cases} \tag{8.16}$$

where we have approximated the line energy $u(\theta = 1)$ in Eq. (6.23) by the critical defect strength U_c. The longitudinal and transverse dimensions of the half loop are

$$L_\parallel \sim \left(\frac{U_R}{\tilde{\epsilon}_1}\right)^{1/2} \frac{c\tilde{\epsilon}_1}{J\phi_0}, \tag{8.17}$$

$$L_\perp \sim \frac{U_R c}{J\phi_0}. \tag{8.18}$$

Equations (8.15), (8.17), and (8.18) are valid when $L_\parallel \gg \ell_\parallel$ and $L_\perp \gg x_G(\ell_\parallel/a)^\zeta$. For large $\ell_\parallel/a$, these conditions are equivalent, and require that $J \ll J_C$, where

$$J_C \sim \frac{U_R c}{\phi_0 x_G} \left(\frac{a}{\ell_\parallel}\right)^\zeta. \tag{8.19}$$

The small-scale results of Ref. 3 can also be taken over. In terms of the parameters of Sec. IIII C, the barrier energy is

$$E_B(L_\parallel \ll \ell_\parallel) \sim E_P \left[\left(\frac{\tilde{\epsilon}_1 a}{E_P}\right)^{1/2} \frac{E_P c}{J\phi_0 a^2}\right]^{\frac{\omega}{1+\zeta-\omega}}. \tag{8.20}$$

The typical scales of the excitations are

$$L_\parallel \sim a \left[\left(\frac{\tilde{\epsilon}_1 a}{E_P}\right)^{1/2} \frac{E_P c}{J\phi_0 a^2}\right]^{\frac{1}{1+\zeta-\omega}}, \tag{8.21}$$

$$L_\perp \sim x_G (L_\parallel/a)^\zeta. \tag{8.22}$$

These point-impurity-like excitations exist for $L_\parallel \ll \ell_\parallel$, or $J \gg J_P$, where

$$J_P \sim \left(\frac{\tilde{\epsilon}_1 a}{E_P}\right)^{1/2} \frac{E_P c}{\phi_0 a^2} \left(\frac{a}{\ell_\parallel}\right)^{1+\zeta-\omega}. \tag{8.23}$$

For the point impurity regime to exist at all, we require $\ell_\parallel \gg a$. In this limit, Eq. (8.16) gives $U_R \sim (a/\ell_\parallel)^{1-\omega} U_c \sim (a/\ell_\parallel)^{1-\omega} E_P/a$. A comparison of Eqs. (8.19) and (8.23) shows that $J_P/J_C = O(1)$. It is therefore possible to define a single crossover current scale $J_{\rm CP} \sim J_C \sim J_P$.

Since the barriers are known, the thermally activated form,

$$\mathcal{E} \sim \rho_0 J \exp\left[-E_B(J)/k_B T\right], \tag{8.24}$$

can be evaluated in the two limits. In both cases, one finds a nonlinear relation,

$$\mathcal{E} \sim \rho_0 J \exp\left[-\left(\frac{J_0}{J}\right)^\mu\right], \tag{8.25}$$

where

$$\mu = \begin{cases} 1, & J \ll J_{\rm CP}, \\ \omega/(1+\zeta-\omega), & J \gg J_{\rm CP}, \end{cases} \tag{8.26}$$

and

$$J_0 = \begin{cases} \frac{U_R}{k_B T}\left(\frac{U_R}{\tilde{\epsilon}_1}\right)^{1/2} \frac{c\tilde{\epsilon}_1}{\phi_0}, & J \ll J_{\rm CP}, \\ \left(\frac{E_P}{k_B T}\right)^{(3-2\omega)/2\omega} \left(\frac{\tilde{\epsilon}_1 a}{E_P}\right)^{1/2} \frac{E_P a}{J\phi_0 a^2}, & J \gg J_{\rm CP}. \end{cases} \tag{8.27}$$

By fitting to these scaling forms, $J_{\rm CP}$ could be determined experimentally and used to extract $\ell_\parallel$.

Another bulk probe which should be able to detect the localization length is neutron scattering. Like the real-time surface imaging, this technology for high-T_c superconductors is still in development.[42] Once on line, however, scattering measurements should reveal some signal of FL localization at wave vectors $q_z \approx 2\pi/\ell_\parallel$.

In lieu of good experimental data, simulations offer another way to test the theory. The zero-temperature numerics of Sec. VII are clearly not sufficiently powerful to settle questions about critical exponents, nor do they address dynamics at the transition. Monte Carlo simulations have been performed on a single FL and a columnar pin without point disorder in Ref. 14. Further simulations along those lines, incorporating bulk randomness, should be possible. Numerically determined I-V char-

acteristics, as well as direct measurements of $\ell_\perp$ and $\ell_\parallel$ through the FL conformations, would shed much light on the issues addressed in this paper.

IX. CONCLUSIONS

The interplay between different types of pinning in type-II superconductors leads to an extremely rich variety of effects. In this paper, we have discussed what is perhaps the simplest such case, the competition between point impurities and a single extended defect for one flux line. For a defect with n extended dimensions, the lower critical dimension d_l satisfies $(d_l - n)\zeta = 1 - \omega$, above which a nontrivial unbinding transition can exist for strong point disorder. This is the case in three dimensions with a columnar pin, leading to the phase diagram in Fig. 4. Several techniques were used to analyze the critical behavior of this transition, the most reliable of which is probably the ϵ expansion. This yields the result $\nu_\perp \approx 1.4$, in good agreement with our numerical simulations, which find $\nu_\perp = 1.3 \pm 0.6$. The best candidate for observation of this effect is in a YBCO sample with widely spaced dislocation lines and a high density of oxygen vacancies, either through nonlinear I-V measurements, surface imaging, or neutron scattering.

A number of other theoretical investigations of some aspects of this problem have appeared recently. Kolomeisky and Straley,[21] using a renormalization-group technique, obtained results for d_l and the critical exponents which agree with ours to lowest order in ϵ, though they find an upper critical dimension $d_u = 4$, at which these exponents lock in to the values given in our Sec. IV. Tang and Lyuksyutov[26] also agree on d_l, and use the Migdal-Kadanoff RG to argue that the coefficient of the Δ^2 term is positive, in agreement with the functional RG result. They also performed numerical simulations in three dimensions, using a mapping of the FL problem to the growth of a driven interface.[11] They find $\nu_\perp = 1.8 \pm 0.6$, which includes our functional RG result. Hwa and Natterman[27] employ a fluctuation-dissipation theorem to develop the RG in two dimensions around the nonperturbative delocalized fixed point. They also find a positive $O(\Delta^2)$ term, leading to our ϵ-expansion result.

Based upon the general agreement of these approaches, we believe the static transition and its critical behavior are now fairly well understood. As pointed out in Sec. VIII, the flux creep becomes nontrivial near the critical point. For larger applied currents, the FL must eventually depin even at zero temperature. Such a depinning transition should be similar to that studied for charge density waves[43] and interfaces.[44]

Once interactions with other flux lines and other extended defects are included, even the statics becomes more complicated. The case of a single FL and a finite density of columnar pins has been studied in Ref. 45. Reference 9 shows that the inclusion of many flux lines does *not* result simply in a Bose glass (though it may appear so up to a very large crossover length scale). Even the physics of many flux lines and many extended defects, such as the so-called "intrinsic" pinning between the CuO planes, *without* point impurities, is quite complex.[46] Certainly the dynamics of such phases is even more rich. We must leave these many questions for the reader.

ACKNOWLEDGMENTS

We acknowledge discussions with D. S. Fisher, T. Natterman, T. Hwa, and D. R. Nelson. This research was supported by the NSF through Grant No. DMR-90-01519, and Harvard University's Materials Research Lab, Grant No. DMR-91-06237.

[1] D. R. Nelson, Phys. Rev. Lett. **60**, 1973 (1988); D. R. Nelson and H. S. Seung, Phys. Rev. B **39**, 9153 (1989).
[2] A. I. Larkin and Y. N. Ovchinikov, J. Low Temp. Phys. **34**, 409 (1979).
[3] M. P. A. Fisher, Phys. Rev. Lett **62**, 1415 (1989); D. S. Fisher, M. P. A. Fisher, and D. A. Huse, Phys. Rev. B **43**, 130 (1991).
[4] L. Civale, A. D. Marwick, T. K. Worthington, M. A. Kirk, J. R. Thompson, L. Krusin-Elbaum, Y. Sum, J. R. Clem, and F. Holtzberg, Phys. Rev. Lett. **67**, 648 (1991).
[5] M. Leghissa, L. A. Gurevich, M. Kraus, G. Saemann-Ischenko, and L. Ya. Vinnikov, Phys. Rev. B **48**, 1341 (1993).
[6] D. R. Nelson and V. M. Vinokur, Phys. Rev. Lett. **68**, 2398 (1992).
[7] D. R. Nelson and V. M. Vinokur, Phys. Rev. B **48**, 13 060 (1993).
[8] M. C. Marchetti and V. M. Vinokur (unpublished).
[9] T. Hwa, D. R. Nelson, and V. M. Vinokur, Phys. Rev. B **48**, 1167 (1993).
[10] L. Balents, Europhys. Lett. **24**, 489 (1993).
[11] M. Kardar and Y.-C. Zhang, Phys. Rev. Lett. **58**, 2087 (1987).
[12] J. Krug and H. Spohn, in *Solids Far From Equilibrium: Growth, Morphology and Defects*, edited by C. Godreche (Cambridge University Press, New York, 1990).
[13] D. S. Fisher and D. A. Huse, Phys. Rev. B **43**, 10 728 (1991).
[14] S. Ryu, A. Kapitulnik, and S. Doniach (unpublished).
[15] L. Balents and M. Kardar, Europhys. Lett. **23**, 503 (1993).
[16] D. S. Fisher, in *Phenomenology and Applications of High Temperature Superconductors—the Los Alamos Symposium, 1991*, edited by K. S. Bedell, M. Inui, D. E. Meltzer, J. R. Schrieffer, and S. Doniach (Addison-Wesley, New York, 1992).
[17] M. Murakami *et al.*, in *Phenomenology and Applications of High Temperature Superconductors—the Los Alamos Symposium, 1991* (Ref. 16).
[18] P. G. DeGennes, *Superconductivity of Metals and Alloys* (W. A. Benjamin, Inc., New York, 1966).
[19] C. J. van der Beek and P. H. Kes, Phys. Rev. B **43**, 13 032 (1991); P. H. Kes, in *Phenomenology and Applications of*

High Temperature Superconductors—the Los Alamos Symposium, 1991 (Ref. 16).
[20] M. E. Fisher, J. Stat. Phys. **34**, 667 (1984).
[21] E. Kolomeisky and J. Straley (unpublished).
[22] E. Medina, T. Hwa, M. Kardar, and Y.-C. Zhang, Phys. Rev. B **39**, 3053 (1989).
[23] D. A. Huse, C. Henley, and D. S. Fisher, Phys. Rev. Lett. **55**, 2924 (1985).
[24] L.-H. Tang, T. Nattermann, and B. M. Forrest, Phys. Rev. Lett. **65**, 2422 (1990).
[25] T. Nattermann and R. Lipowsky, Phys. Rev. Lett. **61**, 2508 (1988).
[26] L.-H. Tang and I. F. Lyuksyutov, Phys. Rev. Lett. **71**, 2745 (1993).
[27] T. Hwa and T. Natterman (unpublished).
[28] R. Lipowsky and M. E. Fisher, Phys. Rev. Lett. **56**, 472 (1986).
[29] See A. N. Berker and S. Ostlund, J. Phys C **12**, 4961 (1979), and references therein.
[30] J. Cook and B. Derrida, J. Stat. Phys. **57**, 89 (1989).
[31] B. Derrida and R. B. Griffiths, Europhys. Lett. **8**, 111 (1989).
[32] T. Halpin-Healy, Phys. Rev. A **42**, 711 (1990).
[33] L. Balents and D. S. Fisher, Phys. Rev. B **48**, 5949 (1993).
[34] C. A. Doty and D. S. Fisher (unpublished).
[35] This can be seen by making the ansatz $V_D(\mathbf{x}, l) = V_{D,1}(\mathbf{x})e^{\lambda l}$, and integrating the resulting equation for $V_{D,1}$ over $\mathbf{x}_\perp$.
[36] M. Kardar, Phys. Rev. Lett **55**, 2235 (1985); Nucl. Phys. B **290**, 582 (1987).
[37] M. Zapotocky and T. Halpin-Healy, Phys. Rev. Lett. **67**, 3463 (1991); J. Wuttke and R. Lipowsky, Phys. Rev. B **44**, 13 042 (1991).
[38] Though the naive estimates of this section would suggest that the FL is stable to kink formation for weak point disorder in $d = 2$, more refined arguments may change this result. Indeed, for the case of many FL's and many columnar pins, Ref. 9 concludes that the Bose glass phase is unstable due to effects from rare regions.
[39] M. Hawley, J. D. Raistrick, J. G. Beery, and R. J. Houlton, Science **251**, 1587 (1991); Ch. Gerber, D. Anselmetti, J. G. Bednorz, J. Mannhart, and D. G. Schlom, Nature **350**, 279 (1991).
[40] See, e.g., P. L. Gammel, D. J. Bishop, G. J. Dolan, J. R. Kwo, C. A. Murray, L. F. Schneemeyer, and J. V. Waszczak, Phys. Rev. Lett. **59**, 2592 (1987); G. J. Dolan, G. V. Chandrashekhar, T. R. Dinger, C. Field, and F. Holtzberg, *ibid.* **62**, 829 (1989).
[41] K. Harada, T. Matsuda, J. Bonevich, M. Igarashi, S. Kondo, G. Possi, U. Kawabe, and A. Tonomura, Nature **360**, 51 (1992).
[42] P. L Gammel, D. A. Huse, R. N. Kleiman, B. Batlogg, C. S. Oglesby, E. Bucher, D. J. Bishop, T. E. Mason, and K. Mortensen Phys. Rev. Lett. **72**, 278 (1994).
[43] O. Narayan and D. S. Fisher, Phys. Rev. Lett. **68**, 3615 (1992); Phys. Rev. B **46**, 11 520 (1992).
[44] T. Natterman, S. Stepanow, L.-H. Tang, and H. Leschhorn, J. Phys. II (France) **2**, 1483 (1992).
[45] J. Krug and T. Halpin-Healy, J. Phys. I (France) **3**, 2179 (1993).
[46] See, e.g., L. Balents and D. R. Nelson (unpublished).

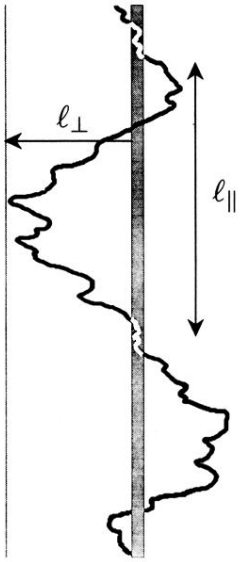

FIG. 1. Flux line localized around a columnar pin in three dimensions ($d = 3$, $n = 1$). White portions of the FL indicate when it is on the defect.

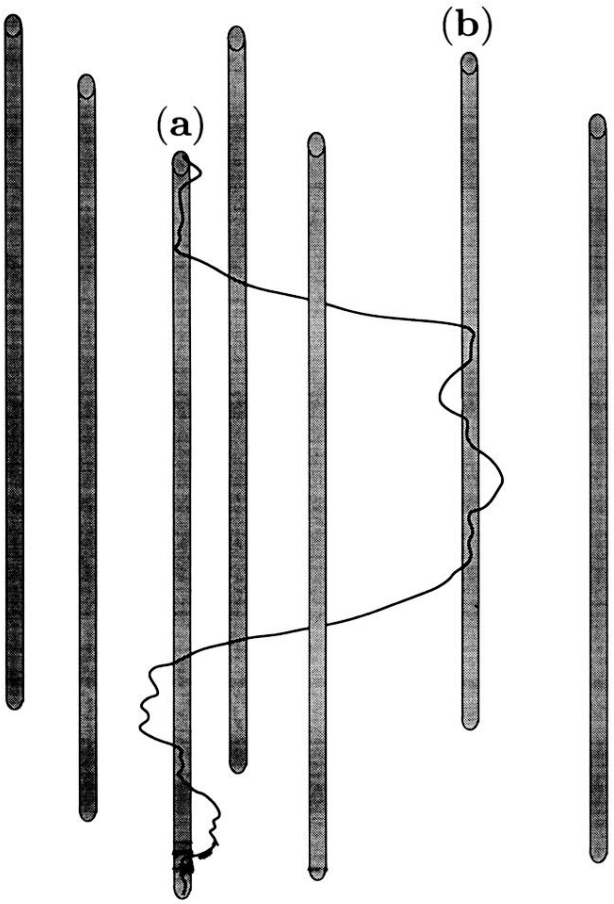

FIG. 17. Single vortex line with many columnar defects. Even though pin (a) has the largest binding energy U_0 energy fluctuations due to point randomness make it favorable for the FL to visit pin (b) by forming a "kink," as shown here.

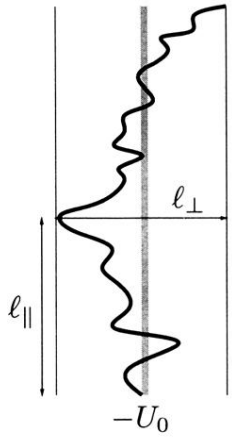

FIG. 2. Schematic illustration of a weakly localized FL. Between regions of width $\ell_\perp$ and height $\ell_\parallel$, the FL must pay an energy cost ($\sim \ell_\perp^{\omega/\zeta}$) to remain localized. This cost is balanced by the loss of energy from the weak defect ($\sim U_0 \ell_\parallel / \ell_\perp^{d-n}$).